Stem Cell Reports
Resource
ISSCR
OPEN ACCESS

Transcriptome Signature and Regulation in Human Somatic Cell Reprogramming

Yoshiaki Tanaka,[1,7] Eriona Hysolli,[1,7] Juan Su,[1,2] Yangfei Xiang,[1] Kun-Yong Kim,[1] Mei Zhong,[3] Yumei Li,[1,4] Kartoosh Heydari,[5] Ghia Euskirchen,[6] Michael P. Snyder,[6] Xinghua Pan,[1] Sherman Morton Weissman,[1] and In-Hyun Park[1,*]
[1]Department of Genetics, Yale Stem Cell Center, Yale School of Medicine, New Haven, CT 06520, USA
[2]Department of Cell Biology, Second Military Medical University, Shanghai 200433, China
[3]Department of Cell Biology, Yale Stem Cell Center, Yale School of Medicine, New Haven, CT 06520, USA
[4]Department of Dermatology, Jiangsu University Affiliated Hospital, Zhenjiang 212000, PRC
[5]Cancer Research Laboratory, LKS Flow Cytometry Facility, University of California, Berkeley, Berkeley, CA 94720, USA
[6]Department of Genetics, Stanford University, Stanford, CA 94305, USA
[7]Co-first author
*Correspondence: inhyun.park@yale.edu
http://dx.doi.org/10.1016/j.stemcr.2015.04.009

SUMMARY

Reprogramming of somatic cells produces induced pluripotent stem cells (iPSCs) that are invaluable resources for biomedical research. Here, we extended the previous transcriptome studies by performing RNA-seq on cells defined by a combination of multiple cellular surface markers. We found that transcriptome changes during early reprogramming occur independently from the opening of closed chromatin by OCT4, SOX2, KLF4, and MYC (OSKM). Furthermore, our data identify multiple spliced forms of genes uniquely expressed at each progressive stage of reprogramming. In particular, we found a pluripotency-specific spliced form of *CCNE1* that is specific to human and significantly enhances reprogramming. In addition, single nucleotide polymorphism (SNP) expression analysis reveals that monoallelic gene expression is induced in the intermediate stages of reprogramming, while biallelic expression is recovered upon completion of reprogramming. Our transcriptome data provide unique opportunities in understanding human iPSC reprogramming.

INTRODUCTION

Induced pluripotent stem cells (iPSCs) have similar properties as embryonic stem cells (ESCs), such as self-renewal and differentiation capacity (Park et al., 2008c; Takahashi and Yamanaka, 2006). Reprogramming technique offers tremendous potential for disease modeling, cell-based therapy, and drug screening (Park et al., 2008a). Although the reprogramming process is quite robust and applicable to various types of adult differentiated cells, only a small fraction of donor cells reaches a fully pluripotent state, while the majority are refractory to reprogramming. Imperfect reprograming may carry somatic memory and may contribute to cancer development (Ohnishi et al., 2014). Therefore, efficient selection and generation of bona fide iPSCs are essential for safe uses in regenerative medicine.

Serial live cell imaging is one of the tools to distinguish bona fide human iPSCs (hiPSCs) from partially reprogrammed cells. Previously, we identified three distinct types of expandable hESC-like colonies during reprogramming via expression patterns of virus-derived GFP, fibroblast marker CD13 (ANPEP), and two pluripotent markers SSEA4 and TRA160 (Chan et al., 2009). Type I cells are defined by continuous expression reprogramming genes ($CD13^{-}GFP^{+}SSEA4^{-}TRA160^{-}$). Type II cells express pluripotency marker SSEA4 and continue expressing reprogramming factors ($CD13^{-}GFP^{+}SSEA4^{+}TRA160^{-}$). Type III cells show expression of TRA160 as well as SSEA4 ($CD13^{-}GFP^{-}SSEA4^{+}TRA160^{+}$). Among these types of colonies, only type III has similar molecular phenotypes with hESCs and become bona fide hiPSCs. Type I and type II cells are partially reprogrammed cells and display negative nuclear NANOG staining, low expression of several pluripotent genes (e.g., *DNMT3B* and *REX1*), and a distinct epigenetic state from type III cells and hESCs. Type I cells remain in their incomplete reprogramed state, while a small population of type II cells may still convert to type III cells and complete hiPSC reprogramming.

Reprogramming pathways have been extensively studied. Mesenchymal-to-epithelial transition (MET) occurs in the initial phase of reprogramming and is synergistically activated by OCT4, SOX2, KLF4, and MYC (OSKM) and BMP signaling, but is blocked by the transforming growth factor β (TGF-β) pathway (Li et al., 2010; Samavarchi-Tehrani et al., 2010). Despite the active function of BMP in the initial reprogramming, BMP proteins prevent the transition of pre-miPSCs to fully reprogrammed miPSCs by maintaining H3K9 methylation (Chen et al., 2013). In contrast, ACTIVIN/NODAL signaling pathway, which is a branch of TGF-β signaling, is essential for mESC self-renewal (Ogawa et al., 2007). WNT ligands and a downstream component of WNT signaling pathway, β-catenin, are required to prevent differentiation and maintain self-renewal in mESCs (Lyashenko et al., 2011). Whereas the transcriptional repressor TCF3 inhibits mESC self-renewal, an interaction with β-catenin followed by WNT3A stimulation activates the expression of self-renewal genes by blocking the TCF3 repressive activity (Yi et al., 2011). A recent study further defined the role of WNT, revealing that this pathway is a negative regulator in the early stages, but switches to a positive regulator in the late stage of mouse reprogramming (Ho et al., 2013).

Transcription profiling during reprogramming has provided critical insights into understanding reprogramming. Microarray-based transcriptome analysis in miPSCs and partially reprogrammed murine cell populations sorted by a fibroblast marker (THY1) and two pluripotent markers (SSEA1 and Oct4-GFP) revealed that the reprogramming process is composed of two main transcriptional waves (Polo et al., 2012). The first wave is driven by Myc and Klf4 and characterized by the loss of fibroblast identity and a gain in cell proliferation. The second wave is controlled by Oct4, Sox2, and Klf4 and is associated with changes in DNA methylation that facilitate stable pluripotency. A microarray and single-cell qPCR study of cell populations sorted by virus-driven EGFP and TRA160 in hiPSC reprogramming, showed that TRA160^{+} cell populations at late time points (approximately day 28) exhibit more similar gene expression patterns to hESCs and less heterogeneous than those at early time points (approximately day 11) (Tanabe et al., 2013). However, most of the nascent TRA160^{+} cells fail to complete reprogramming. These recent reports indicate that transcriptional and signaling regulatory networks are different among intermediate steps.

Here, we set out to investigate the progressive steps of hiPSC reprogramming by *Phi29* DNA polymerase-based mRNA-sequencing (Phi29-mRNA amplification [PMA] RNA-seq) that enables us to monitor transcriptomes in scarce intermediate cell populations (Pan et al., 2013). We identified unique pluripotency-specified spliced transcripts and determined a surprising function of a spliced form of *CCNE* (*pCCNE1*) in improving the reprogramming efficiency. We also found that the actively reprogramming intermediate stage cells acquire a unique ASE pattern, which is erased when reprogramming is completed. Overall, our data analyses allowed us to further dissect the mechanism of hiPSC reprogramming.

RESULTS

Strategy of Transcriptome Profiling from Partially Reprogrammed Cell States

In order to facilitate isolating cells undergoing reprogramming, we initiated reprogramming in human primary fibroblasts with pMSCV-IRES-GFP-based retroviral vectors expressing OSKM (Park et al., 2008b). Cells were harvested at day 3 and weeks 1, 2, 3 and 4 after the viral infection (Figure S1A). The intermediate reprogramed cells from weeks 1 to 4 were further separated by fluorescence-activated cell sorting (FACS) using antibodies for CD13, SSEA4, and TRA160 or GFP expression. At week 1, the majority of cells express virus-derived GFP (Figure S1B), and around 96.9% of those GFP^{+} cells expressed CD13. Double-positive cells (GFP^{+}CD13^{+}) also made up the majority of week 2 cell populations (31.3%), but the ratio of GFP^{+}CD13^{-} cells was greatly increased (20.9%). We observed that 2.7% (GFP^{+}CD13^{-} SSEA4^{+} and GFP^{-}CD13^{-} SSEA4^{+}) of cells at week 2 showed SSEA4 expression with loss of CD13 expression. At weeks 3 and 4, the major cell population consisted of GFP^{+}SSEA4^{-}TRA160^{-} cells (70.0% and 17.5%, respectively), but around 4%–6% of cells displayed expression of two pluripotent markers without GFP expression (GFP^{-}SSEA4^{+}TRA160^{+}). At week 4, colonies showing hESC-like morphology with CD13^{-}GFP^{-}SSEA4^{+}TRA160^{+} cell surface markers were picked for expansion and here on referred to as established iPSCs (grouped together with ESCs in subsequent analyses). PMA RNA-seq was performed in 18 intermediate cell populations, three replicates of parental fibroblasts, fibroblasts at day 3 post-OSKM induction, as well as ESCs and two types of established iPSCs (Pan et al., 2013).

Initial Gene Regulation by OSKM Overexpression in hiPSC Reprogramming

To examine genes immediately regulated by OSKM induction, we compared the transcriptome profile in cells 3 days post-ectopic OSKM overexpression with that of parental fibroblast cells (Figure 1A). Gene Ontology (GO) analysis showed that upregulated genes at day 3 are related to “type I interferon signaling pathway” and “histone modification” (Figure 1B). These genes include *EHMT1*, *EZH2* (Onder et al., 2012), *HMGA1* (Shah et al., 2012), *MED12* (Chia et al., 2010), *RARG* (Wang et al., 2011), and *TAF11* (Maston et al., 2012), which are highly expressed in hESCs and are required for self-renewal, maintenance of pluripotency, or hiPSC reprogramming. Downregulated genes are involved with “cell development” and “TGF-β signaling pathway.” Inhibition of the TGF-β signaling pathway has been characterized and previously shown to enhance iPSC reprogramming (Ichida et al., 2009). These initial responses to OSKM are also detected by reprogramming with electroporation of episomal vectors (Figure S1C). Since the type I interferon pathway is also triggered by the empty vector with infection or electroporation, the induction of this pathway seems to be a general cellular response to foreign viral DNA and not OSKM per se, as both the pMSCV construct and episomal plasmids have been assembled with viral elements (retrovirus and Epstein-Barr virus,

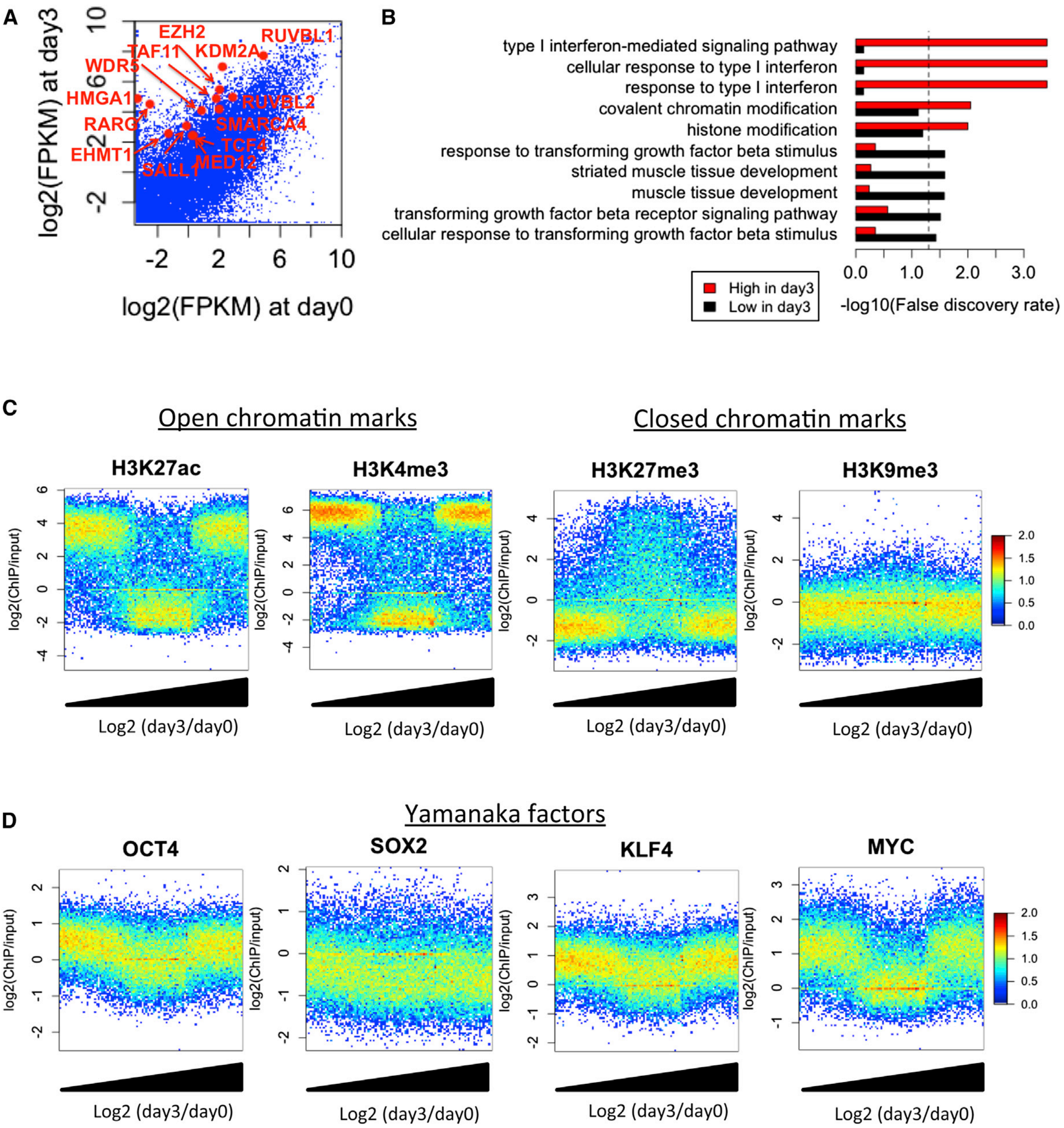

Figure 1. Initial Gene Regulation by OSKM

(A) Comparison of gene expression in OSKM-induced cells between days 0 and 3. Differentially expressed genes (>4-fold) related to "histone modification (GO: 0016570)" or "transcription factor binding (GO: 0008134)" are shown by red dots.

(B) GO analysis of upregulated and downregulated genes at day3. Dashed line represents 0.05 FDR.

(C and D) Comparison of (C) histone modification and (D) OSKM binding level in fibroblast stage with gene expression changes at day3. The x axis represents the rank of genes sorted by increasing order of log2(day 3/day 0) values. The y axis represents log2(ChIP/input). Colors represent log10(count).

See also Figure S1.

respectively). Thus, our data support that the major role of OSKM in the early phase of reprogramming is the activation of reprogramming-related histone remodelers and transcription factors and the suppression of signaling pathways interfering with iPSC reprogramming. This early plasticity, also observed in our 3-day RNA-Seq data, can be utilized to direct differentiation to any lineage of choice (Efe et al., 2011).

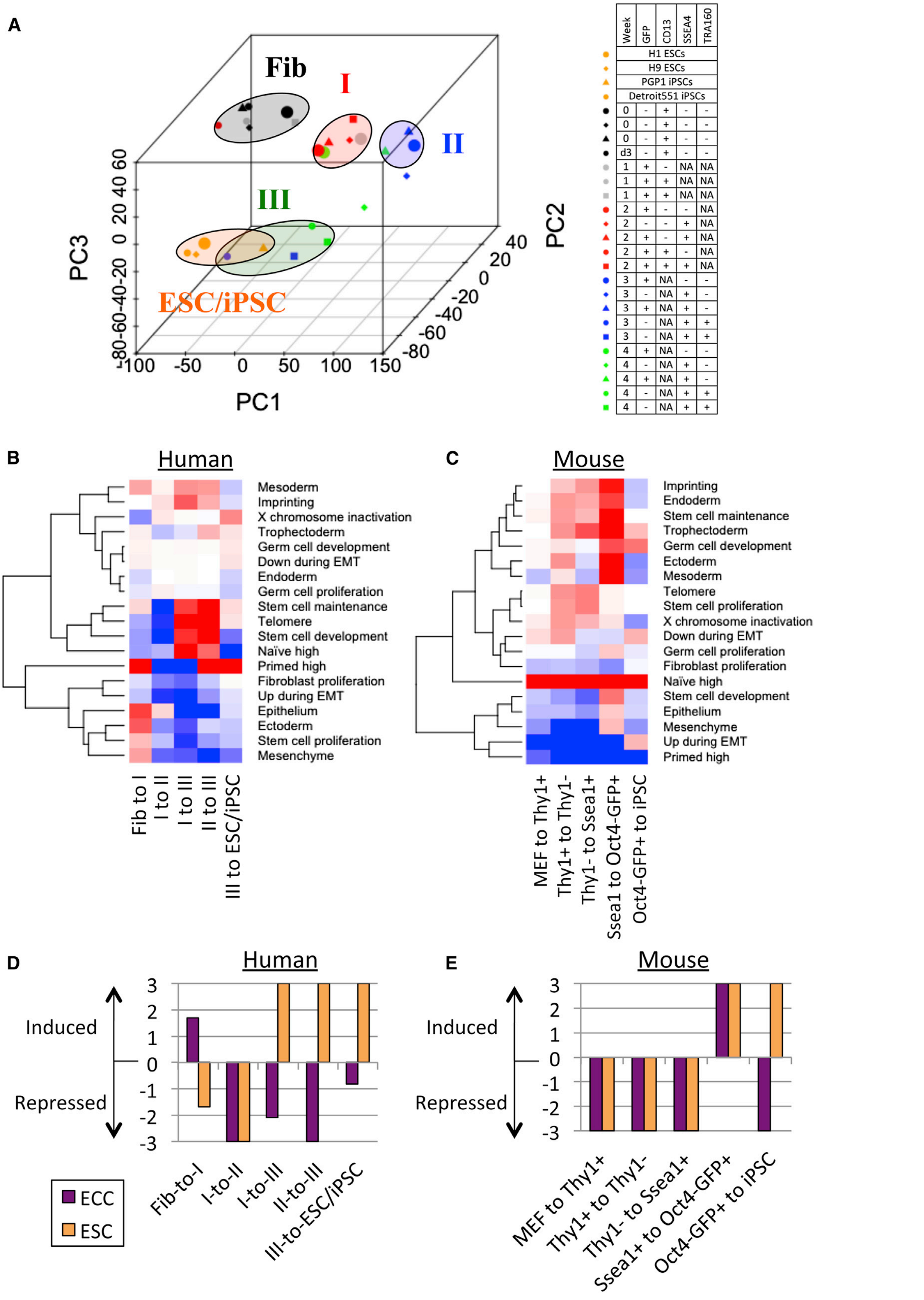

	Week	GFP	CD13	SSEA4	TRA160
●	H1 ESCs				
◆	H9 ESCs				
▲	PGP1 iPSCs				
●	Detroit551 iPSCs				
●	0	-	+	-	-
◆	0	-	+	-	-
▲	0	-	+	-	-
●	d3	-	+	-	-
●	1	+	-	NA	NA
●	1	+	+	NA	NA
■	1	+	+	NA	NA
●	2	+	-	-	NA
◆	2	-	-	+	NA
▲	2	+	-	+	NA
●	2	+	+	-	NA
■	2	+	+	+	NA
●	3	+	NA	-	-
◆	3	-	NA	+	-
▲	3	+	NA	+	-
●	3	-	NA	+	+
■	3	-	NA	+	+
●	4	+	NA	-	-
◆	4	-	NA	+	-
▲	4	+	NA	+	-
●	4	-	NA	+	+
■	4	-	NA	+	+

(legend on next page)

We next asked whether chromatin signatures in the parental fibroblasts and the initial binding of OSKM at promoters determine the genes regulated in the initial phase of reprogramming. To this end, the upregulated and downregulated genes at day 3 were compared with public ChIP-seq studies for histone modifications (Bernstein et al., 2010) and OSKM (Soufi et al., 2012) in fibroblast cells. We did not observe a distinct correlation of the histone modification level and initial OSKM binding between upregulated and downregulated genes at day 3. However, both upregulated and downregulated genes at day 3 showed significantly higher open chromatin marks H3K4me3 and H3K27ac and lower closed chromatin mark H3K27me3 than non-regulated genes (Figure 1C). In addition, OCT4, KLF4, and MYC, but not SOX2, are significantly enriched in both initially regulated promoters (Figure 1D), indicating that genes within pre-existing open chromatin regions are initially regulated by OKM, which act as both activators and repressors.

Transcriptome Analysis Revealed Three Representative Intermediate States during hiPSC Reprogramming

Consistent with our previous classification (Chan et al., 2009), principle component analysis (PCA) segregates the partially reprogrammed cell populations into three distinct stages (types I, II, and III) as well as fibroblast-like and ESC/iPSC stage (Figure 2A). Parental fibroblasts, day 3 reprogrammed cells, and CD13$^+$GFP$^+$ cells at weeks 1 and 2 were grouped into the fibroblast-like stage. Typical type I cells, grouped as type I stage, represented by CD13$^-$GFP$^+$SSEA4$^-$ at weeks 1, 2, and 4, are distinguishable from the fibroblast-like stage, and close to CD13$^+$GFP$^+$SSEA4$^+$, CD13$^-$GFP$^+$SSEA4$^+$, or CD13$^-$GFP$^-$SSEA4$^+$ at week 2, suggesting that repression of the fibroblast phenotype (transition from CD13$^+$ to CD13$^-$) or induction of a pluripotent phenotype (SSEA4$^-$ to SSEA4$^+$) represents the exit from the fibroblast-like stage. Type I cells are the closest to the fibroblast-like stage and neighbor type II and III stages of cells, suggesting that the fibroblast-to-type I transition is the first barrier in the path to iPSCs. Type II stage represents GFP$^+$SSEA4$^+$TRA160$^-$ cell populations and resides closer to type I stage than type III. Type II is the most distant stage from fibroblasts and ESC/iPSCs. Type III stage is composed of GFP$^-$SSEA4$^+$TRA160$^+$ cells and shows the most similar transcriptional patterns with ESCs and iPSCs. Despite the repression of CD13 from the fibroblast-like stage, the expression levels of several other fibroblast markers, such as *COL1A1* and *COL1A2*, are higher in types I and II than ESC/iPSCs. Meanwhile, the expression of these genes in type III cells is as low as that of ESC/iPSCs, indicating that the fibroblast signature still exists in types I and II stage (Figure S1D). GFP$^-$SSEA4$^+$TRA160$^-$ cell populations at weeks 3 and 4 are located between type II and type III stages and are hypothesized to be in the course of transition from types II to III. Between type III and ESC/iPSCs stage, the expression levels of OSKM and the other pluripotency regulators (e.g., *NANOG*) were not significantly different (Table S1). Around 900 genes show significantly higher expression in ESC/iPSC stage compared with type III (Figure S1E) and are overrepresented as “chromatin modifications” and “transcription cofactor activity” (Figure S1F).

Next, our transcriptome data were compared with gene signatures of unsorted and sorted populations (GFP$^+$TRA160$^-$, or TRA160$^+$) from the published work (Tanabe et al., 2013) by gene set enrichment analysis (GSEA) (Table S2A). All of these signatures are significantly induced in the transition from fibroblast-like to type I stage and also are upregulated in later stages (Figure S1G). Gene signatures at mature stages (TRA160$^+$ cells and iPSCs) are significantly enriched in the I-to-III and II-to-III transitions (false discover rate [FDR] < 0.001), but not in the I-to-II, supporting our observations that type III is closer to ESC/iPSC. In the I-to-II transition, only the gene signature at middle time point (day 11) is significantly enriched (FDR < 0.001). The iPSC signature is also induced in III-to-ESC/iPSC transition (FDR $= 0.001$), suggesting that while close to ESC/iPSC, type III cells have not fully completed reprogramming.

Population-based transcriptome analysis provides a more robust quantification of gene expression and has relatively low technical noise and high reproducibility (Marinov et al., 2014). Although it is very useful to flesh out the characteristics of the whole population, we cannot gauge the biological variation between the cells comprising that population. In order to investigate the heterogeneity of the intermediates, we compared our data with single-cell datasets obtained from partially reprogrammed cells (Chung et al., 2014). Consistently, the majority of double-positive cells (SSEA4$^+$TRA160$^+$) and none of SSEA4$^+$TRA160$^-$ and GFP$^+$ cells were classified into type III group (Figures S1H and S1I). While more than 75% of type II cells are

Figure 2. Characterization of Intermediate Stages in hiPSC Reprogramming

(A) PCA classification of the human intermediate states.

(B and C) GSEA of stem cell functions (B) between distinct human intermediate stages and (C) mouse intermediate stages. Gene sets induced or repressed in the transition between two stages (−log10(FDR)) are shown by red and blue color, respectively.

(D and E) GSEA of ECC and ESC-specific genes in (D) human and (E) mouse.

See also Figure S1.

$SSEA4^{+}TRA160^{-}$, more than 60% of type I cells are GFP^{+}, indicating that the sorted-cell populations display heterogeneity, but mainly occupy specific intermediate stages. Overall, our transcriptome data are highly reliable and allow us to understand gene regulation changes during hiPSC reprogramming.

Primed and Naive-State Signatures Are Induced during iPSC Reprogramming

Despite many previous efforts to induce a naive-state in hESCs and hiPSCs (Takashima et al., 2014; Theunissen et al., 2014), it is still unclear whether or when OSKM induction is responsible for naive- and primed-state properties. To address the ground state in intermediate reprogramming stages, we analyzed the enrichment of genes specifically expressed in naive or primed ESCs (Figure 2B; Table S2B). GSEA revealed that primed-state signatures were significantly induced in fibroblast-to-I (FDR = 0.001) and type III-to-ESC/iPSC transition (FDR = 0.001). In contrast, naive-state signatures were significantly enriched in I-to-III (FDR = 0.001) and II-to-III transitions (FDR = 0.017). Significant repression of the primed-state was observed in I-to-II (FDR = 0.001) and I-to-III transitions (FDR = 0.001). These results indicate that type I and ESC/iPSC are biased to the primed state, whereas type III is to naive state. Type II is represented by a large depletion of primed-state signatures and no induction of naive-state signatures. Unlike dynamic changes of naive and primed signatures in human, murine iPSC reprogramming showed across-the-board increase of naive-specific (FDR < 0.001) and decrease of primed-specific genes (FDR < 0.017) in all intermediate stages (Figure 2C) (Polo et al., 2012).

We further addressed the expression changes in genes related to stem cell functions (Figure 2B). Genes related to stem cell maintenance and development and telomere maintenance are significantly induced in I-to-III and II-to-III transitions (FDR < 0.005). These gene sets are significantly depleted in I-to-II transition (FDR < 0.002), indicating that stem cell properties are gained with naive-state induction in type III. Gene sets involved in fibroblast proliferation are significantly suppressed in I-to-II and I-to-III transitions, confirming that type I stage still has fibroblast features. We observed a significant reduction of EMT-upregulated genes in MEF-to-$ThyI^{+}$ transition in mouse (FDR = 0.001) (Figure 2C). On the other hand, we found a significant induction of epithelium developmental genes in fibroblast-to-I transition (FDR = 0.005) and a reduction of EMT-upregulated genes in I-to-II and I-to-III transitions (FDR = 0.003 and 0.001, respectively) in hiPSC reprogramming. This suggests that MET is required in both early and intermediate phases and promotes the exit of human reprogramed cells from the type I stage. Consistent with our previous finding that human female fibroblasts reactivate their inactive X chromosome during hiPSC reprogramming (Kim et al., 2014b), X-chromosome inactivation (XCI)-related genes are significantly repressed in fibroblast-to-I (FDR = 0.047) and are induced in III-to-ESC/iPSC stage (FDR = 0.042).

Cells in Type I Stage Present the Tumorigenic Potential

Since somatic reprogramming is induced by multiple oncogenic factors, the tumorigenic potential of iPSCs is a major concern for using iPSCs in cell therapy. To examine the tumorigenicity of each intermediate stage of reprogramming, we performed GSEA of cancer-related genes (Figure 2D). Since many oncogenes overlap with pluripotent genes, differentially expressed genes between ESCs and embryonic carcinoma cells (ECCs), a malignant counterpart of ESCs, were used as a cancer-related gene set (Table S2D) (Chang et al., 2010; Sperger et al., 2003). In hiPSC reprogramming, we observed that ECC-specific genes are significantly enriched in fibroblast-to-I transition (Figure 2D; FDR = 0.019). Interestingly, ECC-specific genes are significantly depleted in I-to-II, I-to-III, and II-to-III transitions (FDR = 0.001, 0.007, and 0.001, respectively). Additionally, a significant induction of ESC-specific genes was observed in I-to-III and II-to-III transitions (FDR = 0.001 and 0.001, respectively), indicating that type I is more tumorigenic than the other intermediate stages. This is consistent with our previous report demonstrating the formation of poorly differentiated teratomas from type I cells when injected into immunodeficient mice (Chan et al., 2009). In mouse, ECC-specific genes are significantly induced at Oct4-GFP^{+} stage (FDR = 0.001), but are reduced at mature iPSCs (FDR = 0.001) (Figure 2E). Our results show that tumorigenic potential was induced at the early and late stage of iPSC reprogramming in human and mouse, respectively.

Unique Alternative Splicing in Reprogramming

Alternative splicing (AS) is a key event to generate multiple isoforms and functional diversity in proteins. ESC/iPSC- or type III-specific isoforms are hypothesized to modulate the regulation of pluripotency and self-renewal. To identify stage-specific AS events, we compared spliced read alignments among different reprogramming stages (Figure S2A). A total of 636,803 junctions were aligned by our RNA-seq libraries, and about 24.6% of them were matched with splicing sites of RefSeq genes; 47.7% of them were not matched with RefSeq splicing sites, but were observed within RefSeq gene bodies. Spliced junctions within RefSeq genes were further filtered by (1) stage specificity score, (2) gene expression level, and (3) normalized counts of reads spanning the junction (see Experimental Procedures). Finally, a total of 2,342 (0.367%) splice junctions in 774 genes were identified as stage-specific AS candidates

(Figure 3A). These candidates include spliced junctions in known differentiated cell- or ESC-specific isoforms of *FOXP1* and *MBD2* (Gabut et al., 2011; Lu et al., 2014) (Figures S2B and S2C).

In this study, we focused on the function of a previously uncharacterized variant from the *CCNE1* gene. This variant excludes a highly conserved exon 9 of *CCNE1* (Figure S3A), leading to the modification of Cyclin C-terminal (Cyclin_C) domain (Figure 3B). RT-PCR assay confirmed that the exclusion of exon 9 is observed only in pluripotent-cell stages (type III and ESC/iPSC) (*pCCNE1*, pluripotent *CCNE1*) (Figure 3C). In contrast, the known isoform of *CCNE1* (NM_001238) is ubiquitously expressed from fibroblasts to ESC/iPSC stage (*uCCNE1*, ubiquitous *CCNE1*). Since *pCCNE1* is also detectable in reprogramming with somatic cell nuclear transfer, Sendai virus (Figure S3B), episomal vectors (Figure S3C) and polycistronic OSKM lentivirus (Figures S3D and S3E), its induction does not depend on reprogramming methods. Whereas ESC-specific isoforms of *Foxp1* and *Mbd2* were also observed in mESCs (Figures S2B and S2C), exon 9 skipping of *Ccne1* was not detected in mouse embryonic fibroblasts (MEFs), epiblast stem cells (EpiSCs) and ESCs (Figures 3D and 3E), indicating that *pCCNE1* is a human-specific transcript variant.

Despite the high levels of *uCCNE1* and *pCCNE1* in type III stage and ESCs/iPSCs (Figures 3D and S3B–S3E), neither isoform is considerably expressed in fibroblasts after individual or combinatorial OSKM overexpression (Figures S3F and S3G). However, *pCCNE1* expression is significantly increased by *uCCNE1* overexpression (p = 2.21e-4), whereas *pCCNE1* does not affect *uCCNE1* transcription (p = 0.077). These results suggest that the stem cell-specific splicing of *CCNE1* is not an initial target of OSKM; instead, it is most likely controlled by a higher amount of *uCCNE1* and the transcriptional and signaling networks of pluripotency established in mature hiPSCs (Figure S3H).

Given the specificity of *pCCNE1* expression in the pluripotent stage, we next asked about the functional differences between pCCNE1 and uCCNE1. Consistent with our knowledge that CCNE1 is involved in the cell cycle (Honda et al., 2005), overexpression of uCCNE1 significantly accelerates cell proliferation (p = 0.033 by one-side t test; Figure 3F). In contrast, pCCNE1 displays little effect on cell-cycle progression (p = 0.058). Furthermore, pCCNE1 cannot enhance cell proliferation even after OSKM induction (p = 0.312; Figure 3G), indicating that pCCNE1 loses its (if any) functional role in the cell-cycle progression during reprogramming. Interestingly, overexpression of pCCNE1, but not uCCNE1, with OSKM significantly increased the efficiency of hiPSC reprogramming by 4-fold more than OSKM alone (p = 0.022) or empty vector + OSKM (p = 0.022) (Figure 3H), as quantified by alkaline phosphatase (AP) staining. We validated our reprogramming data by double staining iPSCs with pluripotency markers SSEA4 and TRA160 (Figure S3I). Taken together, our results indicate that *pCCNE1* is a newly identified pluripotent spliced form utilized by somatic cells to acquire pluripotency in a cell cycle-independent manner.

Monoallelic Gene Expression Is Uniquely Induced in Reprogramming

Allele-specific expression (ASE) is one of the gene regulatory systems that increase gene variations in a cell. A major change in ASE is known to occur during the pre-implantation development following maternal mRNA loss and paternal genome activation. Zygotic gene activation is induced at four- to eight-cell transition in humans and at one- to two-cell transition in mice (Xue et al., 2013), whereas in the blastocyst, the majority of genes are expressed biallelically. ESCs and differentiated cells display around 65%–80% of biallelic gene expression (Eckersley-Maslin et al., 2014). Despite much interest in its regulation, the ASE change during hiPSC reprogramming has been poorly understood due to the absence of advanced molecular tools. Thus, we measured the heterozygous single nucleotide polymorphism (SNP) expressions in each cell population isolated during reprogramming and calculated ASE ratios (reference:alternative allele expression ratios) for 105 SNPs observed within genes expressed in parental fibroblasts, intermediate stages, and established iPSCs; 68 of 105 SNPs were known SNPs registered in dbSNP Build 132 (Figure 4A). ASE ratios showing symmetric distribution with the highest peak at 0.5 were observed in parental fibroblasts, cell populations expressing fibroblast marker CD13 ($GFP^{+}CD13^{+}$), and iPSCs (Figure 4B), consistent with our previous report (Lee et al., 2009). This indicates that most genes are expressed from both alleles, or cells expressing either allele are equally mixed in these populations. On the other hand, in types I, II, and III-stage cell populations, ASE ratios in several SNPs were increased and decreased closer to 1 or 0, respectively, indicating that either allele is preferentially expressed during hiPSC reprogramming. The bias level of allelic preference is significantly higher in types I, II, and III than the fibroblast stage (Figure 4C; p = 4.14e-3, 4.29e-2, and 6.50e-4, respectively). This ASE bias was also observed in polycistronic vector-based reprogramming, indicating that the occurrence of ASE is not a corollary to individually expressed transgenes (Figure S3J).

To validate ASE during iPSC reprogramming, we selected two SNPs in the *RPN* and *P4HB* genes and analyzed the SNP expression by Sanger sequencing (Figure 4D). These genes were expressed from both alleles (C and T) in parental D551 fibroblast, fibroblast-stage cell population, and iPSCs, while either allele (C or T) was predominantly or preferentially expressed in types I, II, and III. These results

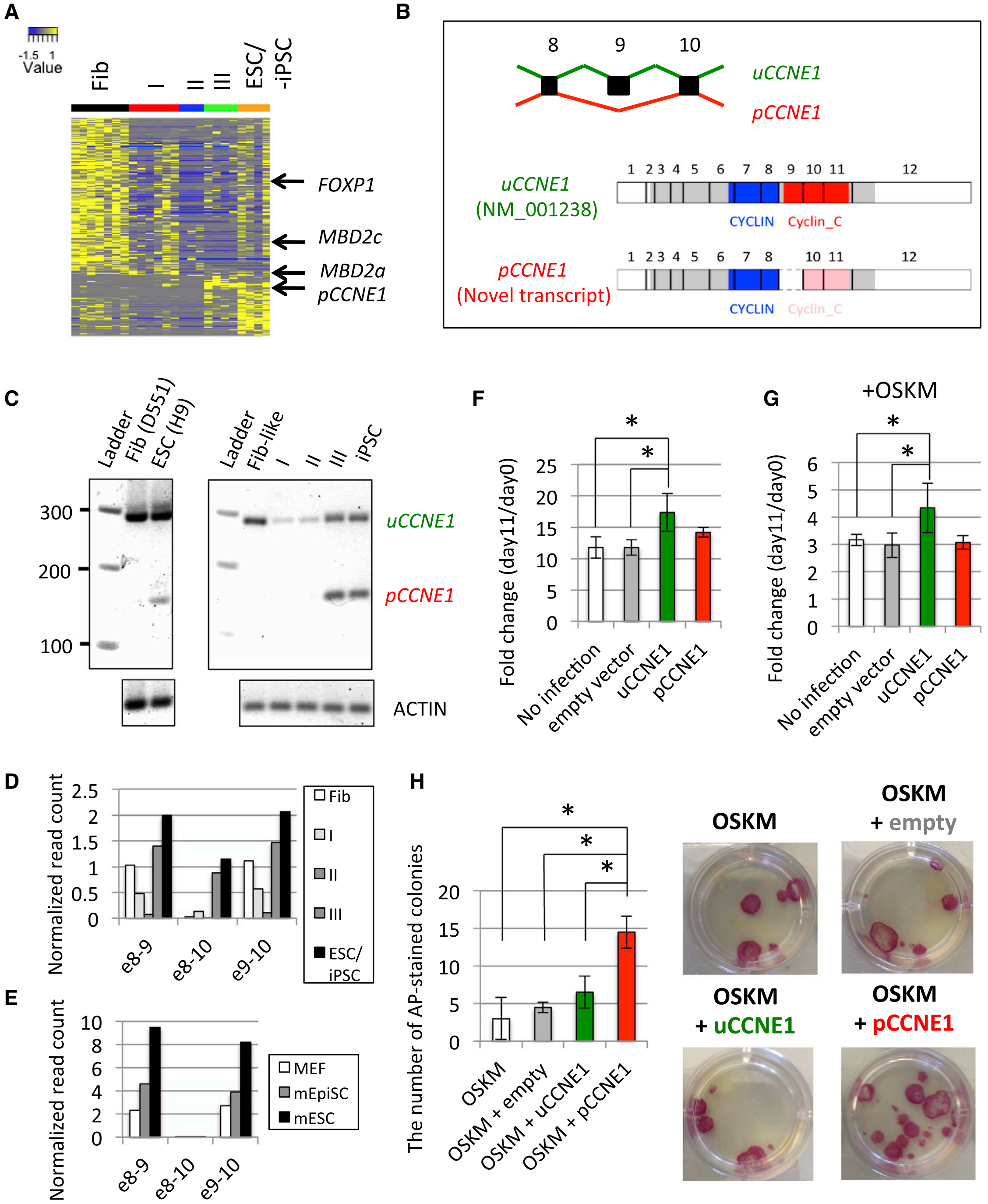

Figure 3. Alternative Spliced Forms of Genes Specific to Each Stage of Reprogramming

(A) Differential expression patterns of splice junctions. Colors represent the normalized read count mapped to each splice junction.

(B) Schematic representation of functional domains of splicing isoforms of *CCNE1*. Gray, blue, and red rectangles represent open reading frame, CYCLIN, and Cyclin_C domain, respectively. Pink rectangles represent the truncated Cyclin_C domain resulting from exon 9 skipping.

(C) RT-PCR assay using primers targeting exons 8 and 10. (Left) is derived from parental fibroblasts and H9 ESCs. (Right) is derived from sorted intermediate populations: Fib-like (w1 CD13$^+$ GFP$^+$), type I (w2 CD13$^+$ GFP$^+$ SSEA4$^+$), II (w4 GFP$^+$ SSEA4$^+$ TRA160$^+$), III (w4 GFP$^-$ SSEA4$^+$ TRA160$^+$), and iPSC.

(D and E) Exon 9 skipping of CCNE1 in (D) human and (E) mouse somatic and pluripotent stem cells.

(legend continued on next page)

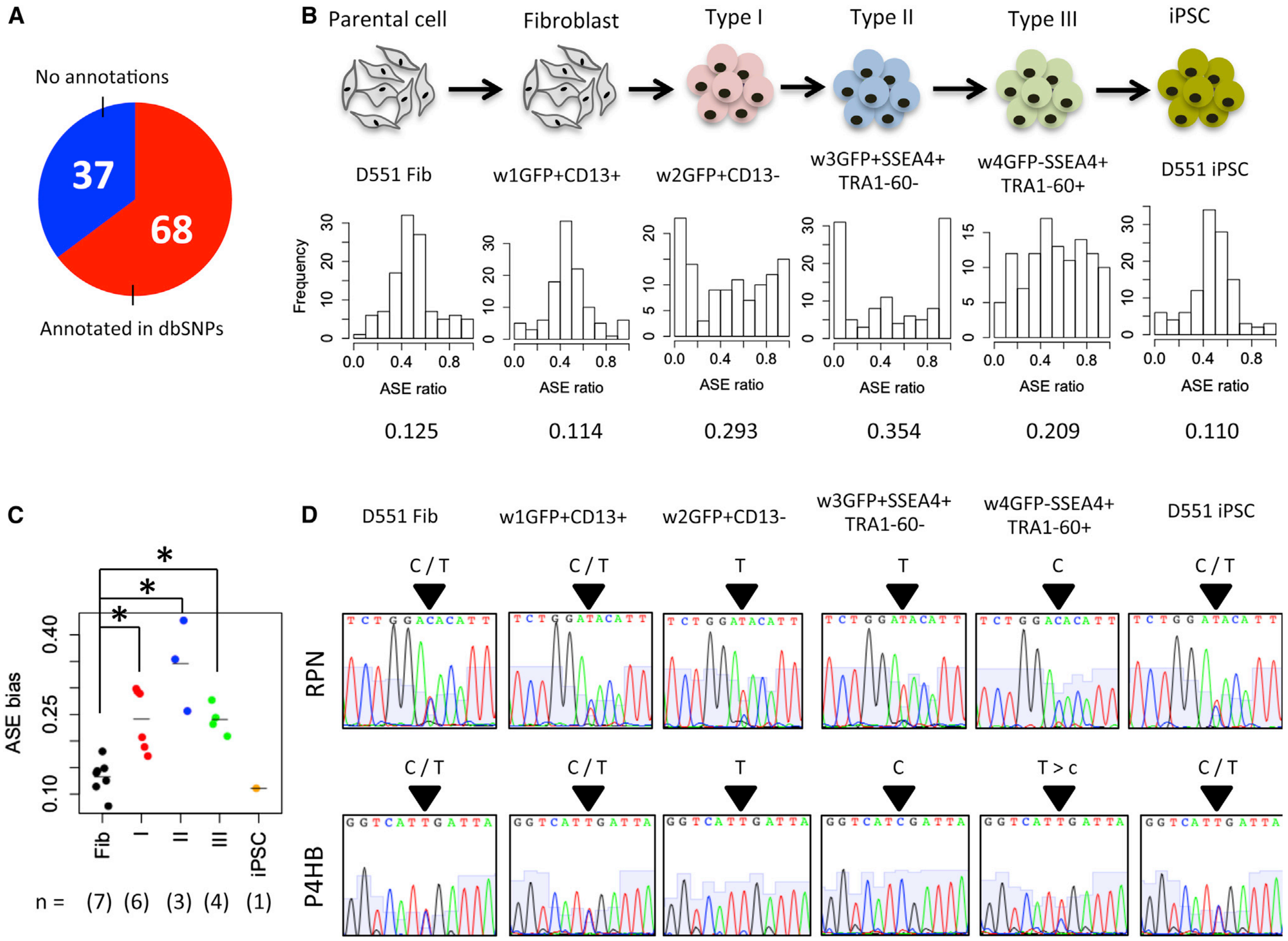

Figure 4. ASE Occurs in Intermediate Stages of hiPSC Reprogramming

(A) Overlap of 105 detected SNPs with dbSNP.

(B) Histograms of ASE ratios in six representative cell populations. Value below histogram represents ASE bias.

(C) Comparison of average ASE bias among different intermediate stages (*$p < 0.05$ by one-sided t test). The number in parentheses denotes the number of populations in each class.

(D) Confirmation of ASE patterns of RPN and P4HB by Sanger sequencing.

See also Figure S3.

indicate that ASE occurs in the intermediate stages and that biallelic expression is restored when cells complete iPSC reprogramming.

Biphasic Change of Signaling Pathways

To gain insight into the mechanisms of signaling pathways in iPSC reprogramming, we analyzed their enrichment at each intermediate stage (Figure 5A; Table S2C). Type I-to-II transition was well represented by the reduction of most signaling pathways, while type II-to-III transition was characterized by the induction of NOTCH and WNT (FDR < 0.042; Figure 5B). Signaling pathways normally reduced or blocked in iPSC reprogramming (p53, neurotrophin, and MAPK) were indeed significantly repressed in

(F and G) Effect of CCNE1 variants on cell growth rate. Fold change of cell count at day 11 to that at day 0 was calculated (F) without and (G) with OSKM induction (*$p < 0.05$ by one-side t test, three biological replicates). Error bars represent SD.

(H) Positive regulation of hiPSC reprogramming by pCCNE1 overexpression. (Right) represents representative AP$^+$ colonies in 12-well plate induced by overexpression of empty vector, uCCNE1, or pCCNE1 with reprogramming factors OSKM (three biological replicates). Error bars represent SD.

See also Figures S2 and S3.

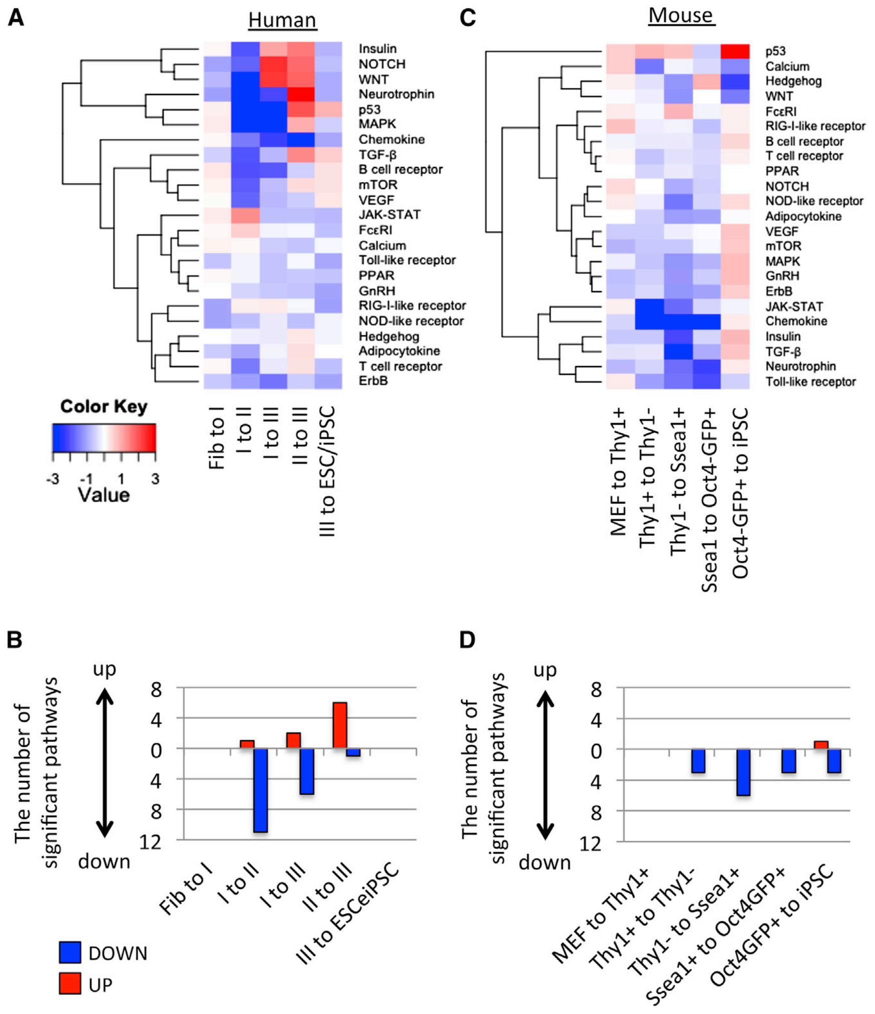

Figure 5. Biphasic Change of Signaling Pathways during hiPSC Reprogramming

(A and B) GSEA of signaling pathways (A) between distinct human intermediate stages and (B) between distinct mouse intermediate stages.

(C and D) The count of significantly upregulated (red) or downregulated (blue) pathways in (C) human and (D) mouse iPSC reprogramming.

See also Figure S4.

I-to-II, I-to-III, and II-to-III transitions (FDR < 0.009) (Hong et al., 2009; Ishizuka et al., 2014; Levenberg et al., 2005). No significant induction or repression of any signaling pathways was observed in fibroblast-to-I and III-to-ESC/iPSC transition.

NOTCH signaling is one of the pathways that display a biphasic change. By adding NOTCH inhibitor DAPT or activator DLL4 ligand at specific periods of reprogramming (Figure S4A), we found that NOTCH inhibition at an early time point and activation at a late time point is more efficient than vice versa in enhancing reprogramming (Figures S4B and S4C). These data suggest that biphasic change of signaling pathway is an important consideration to improve the efficiency of iPSC reprogramming.

Conversely, we found no significant induction in most of signaling pathways between intermediate cells during murine iPSC reprogramming (Figures 5C and 5D). Only the P53 signaling pathway was significantly upregulated in Oct4-GFP$^+$-to-iPSC transition (FDR = 0.001). These results suggest distinct signaling mechanisms during iPSC reprogramming between human and mouse or, alternatively, that hiPSC reprogramming is more sensitive to signaling pathways.

Type III and ESC/iPSC Signatures Are Co-regulated by Multiple Pluripotent Transcription Factors

Developmental genes have high factor loadings (FLs), while genes associated with the cell cycle and stem cell development have low FLs in principle component (PC) 2 and 3 (Figure S5A). Using FLs in PC1-3, we classified genes into three groups that are highly expressed in fibroblast type I (957 genes), type II (123 genes), and III-ESC/iPSC (511 genes) (Figure 6A; Table S3). The fibroblast type I group includes many fibroblast-specific markers such as *CD13*, *COL1A1*, *COL1A2*, and *S100A4*. In contrast, type III-ESC/iPSC group contains known pluripotency genes such as *LIN28A*, *NANOG*, *PRDM14*, *ZFP42* (*REX1*), and *DNMT3B*. The type II group includes genes that both

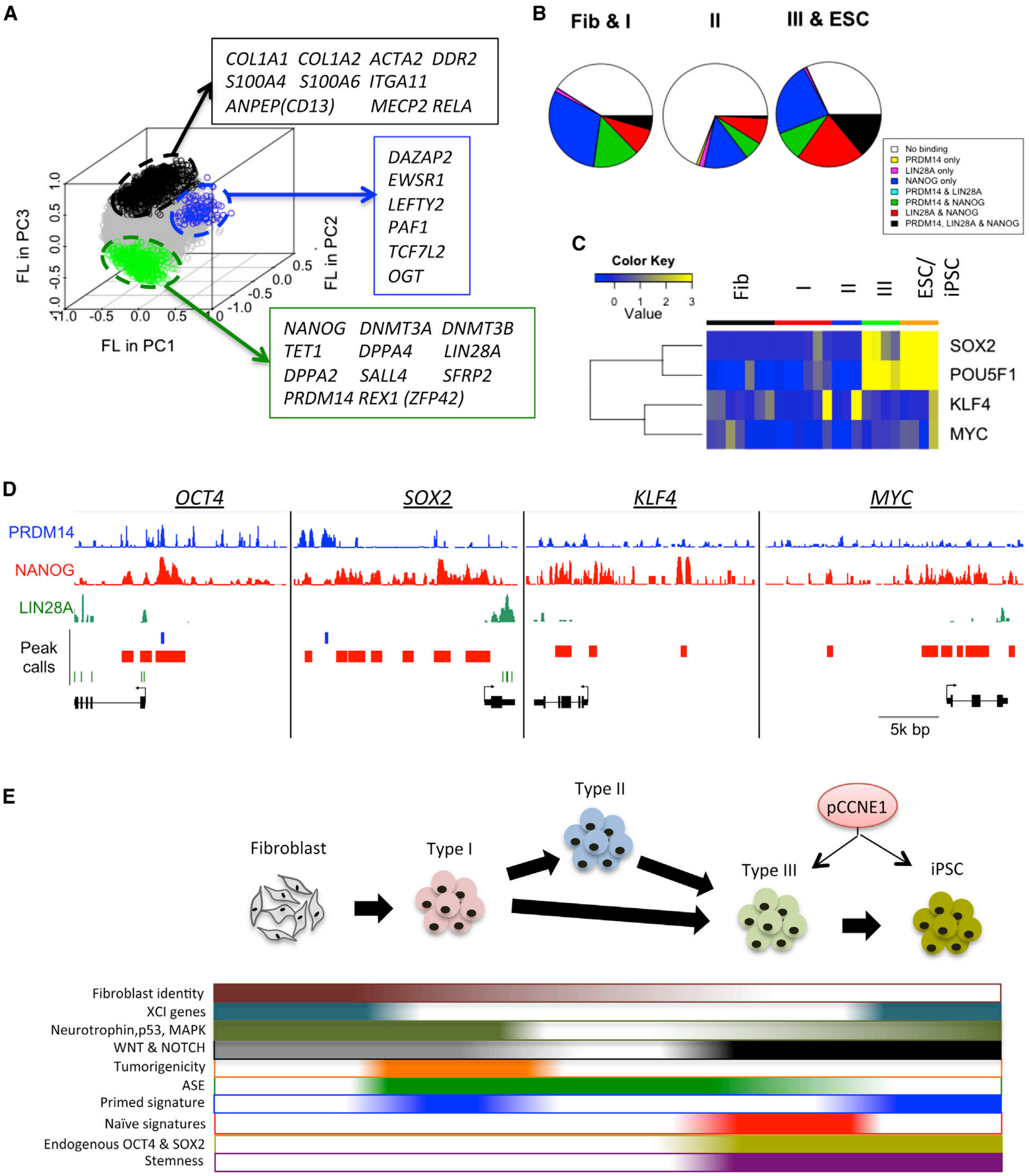

Figure 6. Transcriptional Regulation of Type III and ESC/iPSC Signatures by Multiple Pluripotent Factors

(A) Genes preferentially expressed in fibroblasts and type I, type II, and type III and ESC/iPSC. FLs in PC1–3 of each gene are plotted.

(B) Ratios of NANOG, PRDM14, and LIN28A target genes in fibroblast and type I, type II, and type III and ESC/iPSC gene sets.

(C) Endogenous OSKM expression patterns during hiPSC reprogramming. Relative expression to average was shown by color range blue (low expression) to yellow (high expression).

(D) NANOG, PRDM14, and LIN28A binding patterns in OSKM loci.

(E) Model of reprogramming milestones.

See also Figure S5.

promote (*OGT* and *PAF1*) and block pluripotency and self-renewal (*LEFTY2*) (Ding et al., 2009; Jang et al., 2012; Kim et al., 2014a).

To understand the regulatory mechanism of type III and iPSC gene signatures, we analyzed genes targeted by three main pluripotency regulatory factors (*NANOG*, *PRDM14*, and *LIN28A*) enriched in type III/ESC/iPSCs by using publicly available ChIP-seq and CLIP-seq datasets (Chia et al., 2010; Kunarso et al., 2010; Wilbert et al., 2012). Whereas NANOG binds more than 15,000 gene loci, PRDM14 and LIN28A targets comprise around 5,000 genes (Figure S5B). In addition, more than 95% of LIN28A and PRDM14 targets were co-targeted by NANOG. NANOG targets were significantly enriched in the fibroblast type I (p = 1.20e-12 by hypergeometric test) and type III-ESC/iPSC groups (p = 6.26e-3), but not in type II (p = 0.999) (Figures 6B and S5C). However, unique targets of NANOG are only significantly enriched in the fibroblast type I group (p = 2.86e-5), but not in type II (p = 0.983) and type III-ESC/iPSC groups (p = 0.871), suggesting that the gene regulation of type III-ESC/iPSC group is mediated by co-regulation of NANOG and the other pluripotent factors.

We found that endogenous *OCT4* and *SOX2* RNA expressions are only induced in type III and ESC/iPSCs (Figure 6C; Table S4). Since endogenous *Oct4*, *Sox2*, and *Klf4* are induced in iPSCs and ESCs (Figure S5D), human and mouse employ distinct regulatory mechanisms to establish iPSCs. Co-targets of OCT4 and SOX2 were significantly enriched in type III-ESC/iPSC group (Figure S5E; p = 3.59e-14). These results indicate that the activation of endogenous *OCT4* and *SOX2* is correlated with the induction of type III and ESC/iPSC gene signatures in human. In addition, we found that whereas *MYC* and *KLF4* are targeted by NANOG only, *OCT4* and *SOX2* are co-targeted by NANOG, PRDM14, and LIN28A (Figure 6D), supporting our hypothesis that co-regulation of multiple pluripotent transcription factors is required to regulate type III and iPSC gene signatures.

DISCUSSION

Dissecting the transcriptional landscape of reprogramming represents one of the most straightforward ways to understand cell fate change. Most previous studies performed gene expression profiling in whole population of cells undergoing reprogramming. Only recently, the Yamanaka group described the transcriptome changes during human somatic cell reprogramming by microarray analysis of TRA160 sorted cells (Tanabe et al., 2013). Here, we used RNA-Seq to perform extensive transcriptome analyses of somatic cells undergoing reprogramming based on more elaborate combinatorial staining with CD13, SSEA4, and TRA160 and retroviral GFP.

By analyzing cells 3 days post-reprogramming factor induction, we demonstrated that the earliest gene expression response is independent of chromatin changes induced by OSKM. Although a previous study demonstrated that as pioneer regulators OCT4, SOX2, and KLF4 bind to the closed chromatin regions and initiate chromatin rearrangements (Soufi et al., 2012), our results showed that genes located at the closed chromatin regions do not show large transcriptional differences at day 3. Our observation suggests that 3 days is too short a time to remodel the fibroblast closed chromatin structure by OSK and that the initial gene regulation is mainly controlled by OKM transcriptional regulatory function.

Current transcriptome analysis by RNA-seq identified a large number of splicing variants of genes expressed at progressive stages of reprogramming, in addition to parental fibroblasts and iPSCs. In particular, we found that *CCNE1* expresses human-specific pluripotent splicing variant *pCCNE1* only when cells acquire pluripotency. One of the known functions of CCNE1 involves promoting the entry of G1 to S phase by binding to phospho-cyclin-dependent kinase 2 (pCDK2). Overexpression of a full-length uCCNE1 was not effective in promoting reprogramming, while pCCNE1 improved reprogramming without influencing cell-cycle progression. These data suggest that pCCNE1 possesses a pluripotency-specific function different from the cell-cycle-related general function of uCCNE1. The *pCCNE1* isoform lacks exon 9, which is composed of two α helices and a loop (Figure S3A), and may thus play a role independently of its interaction with pCDK (Honda et al., 2005) and its localization at the centrosome (Matsumoto and Maller, 2004). In addition to *pCCNE1*, a large number of spliced forms of previously uncharacterized genes were identified in our analysis, and our data will be a very useful resource to dissect the regulation of gene splicing during reprogramming and function of genes uniquely spliced at pluripotency.

We found that the transitions of type I to types II and III are accompanied by dramatic changes in multiple signal transduction pathways. Interestingly, the P53 pathway was enriched in type III to ESC/iPSC in human and Oct4-GFP+ to iPSCs in mouse. Initially this finding seems somewhat contradictory, as P53 downregulation has been consistently shown to enhance the reprogramming process. However, at least in the human data, we found enrichment of cell-cycle-related genes, stress response, and DNA repair at later reprogramming stages. Since iPSCs have somatic mutations independently of derivation method as well as chromosomal aberrations of parental origin and from early and late passages (Gore et al., 2011; Johannesson et al., 2014), upregulation of P53 pathway could be a response to counter these genetic changes and maintain DNA integrity. Thus, although the purpose of late P53 induction is unclear at present, our data and previous studies point to one or more combinations of a faster cell cycle, reprogramming itself, original parental aberrations, and culture conditions. Similarly, we identified the biphasic repression and induction of the NOTCH signaling pathway, consistent with a recent report (Ichida et al., 2014). We further validated that activation of NOTCH pathway at a late time point increases reprogramming efficiency. We provide valuable information on the distinct function of signaling factors during different stages of reprogramming in order to more efficiently generate iPSCs.

Overall, our robust transcriptome data in cells undergoing hiPSC reprogramming showed dramatic changes in cell signaling pathways, human-specific AS, and ASE during the progressive cell fate change of fibroblasts to iPSCs (Figure 6E). The data will broaden the knowledge of the reprogramming process and human-specific gene regulation.

EXPERIMENTAL PROCEDURES

Cell Culture

Normal primary fibroblast Detroit 551 were purchased from American Type Culture Collection (CCL-110) and maintained in DMEM high glucose (GIBCO) supplemented with 10% fetal bovine serum (FBS) and penicillin/streptomycin. Human ESCs and iPSCs were cultured on irradiated murine embryonic feeder cells in medium containing DMEM/F12, 20% knockout serum replacement, and 4 ng/ml basic fibroblast growth factor (bFGF).

iPSC Reprogramming and Cell Sorting

The reprogramming procedure was conducted as previously described (Park et al., 2008b). Detroit 551 cells were seeded at 100,000 cells/well of a six-well plate 1 day prior to infection. A retrovirus cocktail containing OSKM was added to each well at MOI 5. On day 5 post-infection, the cells were trypsinized and transferred to 10-cm culture dishes containing MEFs. Prior to sorting, the cells were detached using accutase, washed, and incubated in 20% FBS in 1× PBS with the following antibodies according to manufacturer's recommended dilutions: anti-human CD13 (BD catalog number 555394), anti-human/mouse SSEA4 (R&D catalog number FAB1435A), anti-human TRA160 (BD catalog number 560193). Sorting was conducted using a BD FACSAria cell sorter. Then the cells were pelleted and quickly frozen in liquid nitrogen or sorted directly in RLT + 2-mercaptoethanol lysis buffer (QIAGEN).

PMA RNA-Seq Library Construction and Illumina Sequencing

PMA RNA-seq library was prepared as previously described (Pan et al., 2013). Reads mapped to hg19 human genome were used for subsequent analyses. The details are given in Supplemental Experimental Procedures. All public data used in this study were summarized in Table S5.

Gene Expression Analysis

RNA was isolated using an RNeasy minikit (QIAGEN) and used for reverse transcription with iScript (BioRad) according to the manufacturer's protocol with primer sets in Table S6.

ACCESSION NUMBERS

The accession number for the pCCNE1 reported in this paper is GenBank: KR134287. All data are deposited to GEO with accession number GEO: GSE67915.

SUPPLEMENTAL INFORMATION

Supplemental Information includes Supplemental Experimental Procedures, four figures, and six tables and can be found with this article online at http://dx.doi.org/10.1016/j.stemcr.2015.04.009.

AUTHOR CONTRIBUTIONS

Y.T. performed all bioinformatics analysis. E.H. planned and conducted most of the experiments. Y.T., J.S., Y.X., K.-Y.K, and K.H. performed some of the experiments. E.H., Y.L., M.Z., X.P., S.M.W., G.E., and M.S. were involved in designing, generating, and performing PMA RNA-seq. I.-H.P. conceived and coordinated the project. Y.T., E.H., J.S. and I.-H.P. wrote the manuscript.

ACKNOWLEDGMENTS

I.-H. P. was partly supported by NIH (GM0099130-01, GM111667-01), CSCRF (12-SCB-YALE-11, 13-SCB-YALE-06), KRIBB/KRCF research initiative program (NAP-09-3), and CTSA Grant UL1 RR025750 from the National Center for Advancing Translational Science (NCATS), a component of the NIH, and NIH roadmap for Medical Research. Its contents are solely the responsibility of the authors and do not necessarily represent the official view of NIH. Computation time was provided by Yale University Biomedical High Performance Computing Center.

Received: October 10, 2014
Revised: April 20, 2015
Accepted: April 22, 2015
Published: May 21, 2015

REFERENCES

Bernstein, B.E., Stamatoyannopoulos, J.A., Costello, J.F., Ren, B., Milosavljevic, A., Meissner, A., Kellis, M., Marra, M.A., Beaudet, A.L., Ecker, J.R., et al. (2010). The NIH Roadmap Epigenomics Mapping Consortium. Nat. Biotechnol. *28*, 1045–1048.

Chan, E.M., Ratanasirintrawoot, S., Park, I.H., Manos, P.D., Loh, Y.H., Huo, H., Miller, J.D., Hartung, O., Rho, J., Ince, T.A., et al. (2009). Live cell imaging distinguishes bona fide human iPS cells from partially reprogrammed cells. Nat. Biotechnol. *27*, 1033–1037.

Chang, G., Miao, Y.L., Zhang, Y., Liu, S., Kou, Z., Ding, J., Chen, D.Y., Sun, Q.Y., and Gao, S. (2010). Linking incomplete reprogramming to the improved pluripotency of murine embryonal carcinoma cell-derived pluripotent stem cells. PLoS ONE *5*, e10320.

Chen, J., Liu, H., Liu, J., Qi, J., Wei, B., Yang, J., Liang, H., Chen, Y., Chen, J., Wu, Y., et al. (2013). H3K9 methylation is a barrier during somatic cell reprogramming into iPSCs. Nat. Genet. *45*, 34–42.

Chia, N.Y., Chan, Y.S., Feng, B., Lu, X., Orlov, Y.L., Moreau, D., Kumar, P., Yang, L., Jiang, J., Lau, M.S., et al. (2010). A genome-wide RNAi screen reveals determinants of human embryonic stem cell identity. Nature *468*, 316–320.

Chung, K.M., Kolling, F.W., 4th, Gajdosik, M.D., Burger, S., Russell, A.C., and Nelson, C.E. (2014). Single cell analysis reveals the stochastic phase of reprogramming to pluripotency is an ordered probabilistic process. PLoS ONE *9*, e95304.

Ding, L., Paszkowski-Rogacz, M., Nitzsche, A., Slabicki, M.M., Heninger, A.K., de Vries, I., Kittler, R., Junqueira, M., Shevchenko, A., Schulz, H., et al. (2009). A genome-scale RNAi screen for Oct4 modulators defines a role of the Paf1 complex for embryonic stem cell identity. Cell Stem Cell *4*, 403–415.

Eckersley-Maslin, M.A., Thybert, D., Bergmann, J.H., Marioni, J.C., Flicek, P., and Spector, D.L. (2014). Random monoallelic gene expression increases upon embryonic stem cell differentiation. Dev. Cell *28*, 351–365.

Efe, J.A., Hilcove, S., Kim, J., Zhou, H., Ouyang, K., Wang, G., Chen, J., and Ding, S. (2011). Conversion of mouse fibroblasts into cardiomyocytes using a direct reprogramming strategy. Nat. Cell Biol. *13*, 215–222.

Gabut, M., Samavarchi-Tehrani, P., Wang, X., Slobodeniuc, V., O'Hanlon, D., Sung, H.K., Alvarez, M., Talukder, S., Pan, Q., Mazzoni, E.O., et al. (2011). An alternative splicing switch regulates embryonic stem cell pluripotency and reprogramming. Cell *147*, 132–146.

Gore, A., Li, Z., Fung, H.L., Young, J.E., Agarwal, S., Antosiewicz-Bourget, J., Canto, I., Giorgetti, A., Israel, M.A., Kiskinis, E., et al. (2011). Somatic coding mutations in human induced pluripotent stem cells. Nature *471*, 63–67.

Ho, R., Papp, B., Hoffman, J.A., Merrill, B.J., and Plath, K. (2013). Stage-specific regulation of reprogramming to induced pluripotent stem cells by Wnt signaling and T cell factor proteins. Cell Rep. *3*, 2113–2126.

Honda, R., Lowe, E.D., Dubinina, E., Skamnaki, V., Cook, A., Brown, N.R., and Johnson, L.N. (2005). The structure of cyclin E1/CDK2: implications for CDK2 activation and CDK2-independent roles. EMBO J. *24*, 452–463.

Hong, H., Takahashi, K., Ichisaka, T., Aoi, T., Kanagawa, O., Nakagawa, M., Okita, K., and Yamanaka, S. (2009). Suppression of induced pluripotent stem cell generation by the p53-p21 pathway. Nature *460*, 1132–1135.

Ichida, J.K., Blanchard, J., Lam, K., Son, E.Y., Chung, J.E., Egli, D., Loh, K.M., Carter, A.C., Di Giorgio, F.P., Koszka, K., et al. (2009). A small-molecule inhibitor of tgf-Beta signaling replaces sox2 in reprogramming by inducing nanog. Cell Stem Cell *5*, 491–503.

Ichida, J.K., Tcw, J., Williams, L.A., Carter, A.C., Shi, Y., Moura, M.T., Ziller, M., Singh, S., Amabile, G., Bock, C., et al. (2014). Notch inhibition allows oncogene-independent generation of iPS cells. Nat. Chem. Biol. *10*, 632–639.

Ishizuka, T., Goshima, H., Ozawa, A., and Watanabe, Y. (2014). Involvement of β-adrenoceptors in the differentiation of human induced pluripotent stem cells into mesodermal progenitor cells. Eur. J. Pharmacol. *740*, 28–34.

Jang, H., Kim, T.W., Yoon, S., Choi, S.Y., Kang, T.W., Kim, S.Y., Kwon, Y.W., Cho, E.J., and Youn, H.D. (2012). O-GlcNAc regulates pluripotency and reprogramming by directly acting on core components of the pluripotency network. Cell Stem Cell *11*, 62–74.

Johannesson, B., Sagi, I., Gore, A., Paull, D., Yamada, M., Golan-Lev, T., Li, Z., LeDuc, C., Shen, Y., Stern, S., et al. (2014). Comparable frequencies of coding mutations and loss of imprinting in human pluripotent cells derived by nuclear transfer and defined factors. Cell Stem Cell *15*, 634–642.

Kim, D.K., Cha, Y., Ahn, H.J., Kim, G., and Park, K.S. (2014a). Lefty1 and lefty2 control the balance between self-renewal and pluripotent differentiation of mouse embryonic stem cells. Stem Cells Dev. *23*, 457–466.

Kim, K.Y., Hysolli, E., Tanaka, Y., Wang, B., Jung, Y.W., Pan, X., Weissman, S.M., and Park, I.H. (2014b). X Chromosome of female cells shows dynamic changes in status during human somatic cell reprogramming. Stem Cell Reports *2*, 896–909.

Kunarso, G., Chia, N.Y., Jeyakani, J., Hwang, C., Lu, X., Chan, Y.S., Ng, H.H., and Bourque, G. (2010). Transposable elements have rewired the core regulatory network of human embryonic stem cells. Nat. Genet. *42*, 631–634.

Lee, J.H., Park, I.H., Gao, Y., Li, J.B., Li, Z., Daley, G.Q., Zhang, K., and Church, G.M. (2009). A robust approach to identifying tissue-specific gene expression regulatory variants using personalized human induced pluripotent stem cells. PLoS Genet. *5*, e1000718.

Levenberg, S., Burdick, J.A., Kraehenbuehl, T., and Langer, R. (2005). Neurotrophin-induced differentiation of human embryonic stem cells on three-dimensional polymeric scaffolds. Tissue Eng. *11*, 506–512.

Li, R., Liang, J., Ni, S., Zhou, T., Qing, X., Li, H., He, W., Chen, J., Li, F., Zhuang, Q., et al. (2010). A mesenchymal-to-epithelial transition initiates and is required for the nuclear reprogramming of mouse fibroblasts. Cell Stem Cell *7*, 51–63.

Lu, Y., Loh, Y.H., Li, H., Cesana, M., Ficarro, S.B., Parikh, J.R., Salomonis, N., Toh, C.X., Andreadis, S.T., Luckey, C.J., et al. (2014). Alternative splicing of MBD2 supports self-renewal in human pluripotent stem cells. Cell Stem Cell *15*, 92–101.

Lyashenko, N., Winter, M., Migliorini, D., Biechele, T., Moon, R.T., and Hartmann, C. (2011). Differential requirement for the dual functions of β-catenin in embryonic stem cell self-renewal and germ layer formation. Nat. Cell Biol. *13*, 753–761.

Marinov, G.K., Williams, B.A., McCue, K., Schroth, G.P., Gertz, J., Myers, R.M., and Wold, B.J. (2014). From single-cell to cell-pool transcriptomes: stochasticity in gene expression and RNA splicing. Genome Res. *24*, 496–510.

Maston, G.A., Zhu, L.J., Chamberlain, L., Lin, L., Fang, M., and Green, M.R. (2012). Non-canonical TAF complexes regulate active promoters in human embryonic stem cells. eLife *1*, e00068.

Matsumoto, Y., and Maller, J.L. (2004). A centrosomal localization signal in cyclin E required for Cdk2-independent S phase entry. Science *306*, 885–888.

Ogawa, K., Saito, A., Matsui, H., Suzuki, H., Ohtsuka, S., Shimosato, D., Morishita, Y., Watabe, T., Niwa, H., and Miyazono, K. (2007). Activin-Nodal signaling is involved in propagation of mouse embryonic stem cells. J. Cell Sci. *120*, 55–65.

Ohnishi, K., Semi, K., Yamamoto, T., Shimizu, M., Tanaka, A., Mitsunaga, K., Okita, K., Osafune, K., Arioka, Y., Maeda, T., et al. (2014). Premature termination of reprogramming in vivo leads to cancer development through altered epigenetic regulation. Cell *156*, 663–677.

Onder, T.T., Kara, N., Cherry, A., Sinha, A.U., Zhu, N., Bernt, K.M., Cahan, P., Marcarci, B.O., Unternaehrer, J., Gupta, P.B., et al. (2012). Chromatin-modifying enzymes as modulators of reprogramming. Nature *483*, 598–602.

Pan, X., Durrett, R.E., Zhu, H., Tanaka, Y., Li, Y., Zi, X., Marjani, S.L., Euskirchen, G., Ma, C., Lamotte, R.H., et al. (2013). Two methods for full-length RNA sequencing for low quantities of cells and single cells. Proc. Natl. Acad. Sci. USA *110*, 594–599.

Park, I.H., Arora, N., Huo, H., Maherali, N., Ahfeldt, T., Shimamura, A., Lensch, M.W., Cowan, C., Hochedlinger, K., and Daley, G.Q. (2008a). Disease-specific induced pluripotent stem cells. Cell *134*, 877–886.

Park, I.H., Lerou, P.H., Zhao, R., Huo, H., and Daley, G.Q. (2008b). Generation of human-induced pluripotent stem cells. Nat. Protoc. *3*, 1180–1186.

Park, I.H., Zhao, R., West, J.A., Yabuuchi, A., Huo, H., Ince, T.A., Lerou, P.H., Lensch, M.W., and Daley, G.Q. (2008c). Reprogramming of human somatic cells to pluripotency with defined factors. Nature *451*, 141–146.

Polo, J.M., Anderssen, E., Walsh, R.M., Schwarz, B.A., Nefzger, C.M., Lim, S.M., Borkent, M., Apostolou, E., Alaei, S., Cloutier, J., et al. (2012). A molecular roadmap of reprogramming somatic cells into iPS cells. Cell *151*, 1617–1632.

Samavarchi-Tehrani, P., Golipour, A., David, L., Sung, H.K., Beyer, T.A., Datti, A., Woltjen, K., Nagy, A., and Wrana, J.L. (2010). Functional genomics reveals a BMP-driven mesenchymal-to-epithelial transition in the initiation of somatic cell reprogramming. Cell Stem Cell *7*, 64–77.

Shah, S.N., Kerr, C., Cope, L., Zambidis, E., Liu, C., Hillion, J., Belton, A., Huso, D.L., and Resar, L.M. (2012). HMGA1 reprograms somatic cells into pluripotent stem cells by inducing stem cell transcriptional networks. PLoS ONE *7*, e48533.

Soufi, A., Donahue, G., and Zaret, K.S. (2012). Facilitators and impediments of the pluripotency reprogramming factors' initial engagement with the genome. Cell *151*, 994–1004.

Sperger, J.M., Chen, X., Draper, J.S., Antosiewicz, J.E., Chon, C.H., Jones, S.B., Brooks, J.D., Andrews, P.W., Brown, P.O., and Thomson, J.A. (2003). Gene expression patterns in human embryonic stem cells and human pluripotent germ cell tumors. Proc. Natl. Acad. Sci. USA *100*, 13350–13355.

Takahashi, K., and Yamanaka, S. (2006). Induction of pluripotent stem cells from mouse embryonic and adult fibroblast cultures by defined factors. Cell *126*, 663–676.

Takashima, Y., Guo, G., Loos, R., Nichols, J., Ficz, G., Krueger, F., Oxley, D., Santos, F., Clarke, J., Mansfield, W., et al. (2014). Resetting transcription factor control circuitry toward ground-state pluripotency in human. Cell *158*, 1254–1269.

Tanabe, K., Nakamura, M., Narita, M., Takahashi, K., and Yamanaka, S. (2013). Maturation, not initiation, is the major roadblock during reprogramming toward pluripotency from human fibroblasts. Proc. Natl. Acad. Sci. USA *110*, 12172–12179.

Theunissen, T.W., Powell, B.E., Wang, H., Mitalipova, M., Faddah, D.A., Reddy, J., Fan, Z.P., Maetzel, D., Ganz, K., Shi, L., et al. (2014). Systematic identification of culture conditions for induction and maintenance of naive human pluripotency. Cell Stem Cell *15*, 471–487.

Wang, W., Yang, J., Liu, H., Lu, D., Chen, X., Zenonos, Z., Campos, L.S., Rad, R., Guo, G., Zhang, S., et al. (2011). Rapid and efficient reprogramming of somatic cells to induced pluripotent stem cells by retinoic acid receptor gamma and liver receptor homolog 1. Proc. Natl. Acad. Sci. USA *108*, 18283–18288.

Wilbert, M.L., Huelga, S.C., Kapeli, K., Stark, T.J., Liang, T.Y., Chen, S.X., Yan, B.Y., Nathanson, J.L., Hutt, K.R., Lovci, M.T., et al. (2012). LIN28 binds messenger RNAs at GGAGA motifs and regulates splicing factor abundance. Mol. Cell *48*, 195–206.

Xue, Z., Huang, K., Cai, C., Cai, L., Jiang, C.Y., Feng, Y., Liu, Z., Zeng, Q., Cheng, L., Sun, Y.E., et al. (2013). Genetic programs in human and mouse early embryos revealed by single-cell RNA sequencing. Nature *500*, 593–597.

Yi, F., Pereira, L., Hoffman, J.A., Shy, B.R., Yuen, C.M., Liu, D.R., and Merrill, B.J. (2011). Opposing effects of Tcf3 and Tcf1 control Wnt stimulation of embryonic stem cell self-renewal. Nat. Cell Biol. *13*, 762–770.

Stem Cell Reports

Supplemental Information

Transcriptome Signature and Regulation in Human Somatic Cell Reprogramming

Yoshiaki Tanaka, Eriona Hysolli, Juan Su, Yangfei Xiang, Kun-Yong Kim, Mei Zhong, Yumei Li, Kartoosh Heydari, Ghia Euskirchen, Michael P. Snyder, Xinghua Pan, Sherman Morton Weissman, and In-Hyun Park

SUPPLEMENTAL FIGURE LEGENDS

Figure S1. Transcriptome profiling of intermediate states during hiPSC reprogramming.
(A) Schematic diagram illustrating the processing of human reprogramming intermediates.
(B) Cell counts of intermediate cell populations collected by FACS sorting. The percentage represents the number of cells expressing fibroblast or pluripotent markers calculated by Flowjo vX 0.7 software. The number represents the cell count recovered from FACS.
(C) GSEA of GO biological processes between day 0 and 3 after introduction of episomal vectors (pEP4 E02S ET2K, pEP4 E02S EN2L and pCEP4-M2L) and empty transfected or infected retroviral vector. –log10(FDR) and log10(FDR) of up- and down-regulated gene sets are shown, respectively. * FDR < 0.05.
(D) Fibroblast marker expression in each intermediate stage. Y-axis represents relative gene expression normalized to fibroblasts. Each class is composed of seven (Fib), six (I), three (II), four (III) and four populations (ESC/iPSC).
(E) Heatmap represents differentially-expressed genes ($p<0.05$ by T test and 1.5 fold change) between type III and ESC/iPSC. Relative expression values to the median expression values across eight libraries with log2 scale are represented by green (low expression) and red (high expression) colors.
(F) Overrepresentation of GO terms is shown by bar plot. Dashed line represents 0.05 FDR.
(G) GSEA of differentially-expressed genes in distinct cell populations in (Tanabe et al., 2013) was applied to transition pairs of distinct reprogramming stages. If gene sets are upregulated, -log10(FDR) is shown in red. If gene sets are downregulated, log10(FDR) is shown in blue.
(H) Principle component analysis of single-cell qPCR data.
(I) Percentage of intermediate stages in each cell population.

Figure S2. Identification of ESC-specific alternative splicing (AS) by our transcriptome dataset.
(A) Overview of pipeline to identify alternative splicing.
(B-C) Identification of known ESC-specific transcript variants, (B) *MBD2* and (C) *FOXP1* in human and mouse ESCs. These variants are specifically expressed in human type III-stage cells, iPSCs, and human and mouse ESCs.

Figure S3. Characterization of pCCNE1 isoform and ASE.
(A) Exon 9 of *CCNE1* is highly conserved among vertebrates. CCNE1 protein sequences were aligned by ClustalW2 in EMBL-EBI. Protein sequences coded by exon 9 are shown by black arrow. α-helix structure and centrosomal localization signal sequence were represented by red and blue line, respectively.
(B) Exon 9 skipping of *CCNE1* in parental human dermal fibroblast (HDF, gray), nuclear transfer stem cell (NT, purple), hESC (red), retrovirus-derived iPSCs (iPSC-R, blue) and Sendai virus-derived iPSCs (iPSC-S, green) (Ma et al., 2014).
(C) Expression of *uCCNE1* and *pCCNE1* in transgene-free iPSCs (Lister et al., 2011).
(D) Exon 9 skipping of *CCNE1* in polycistronic vector-derived iPSCs (Friedli et al., 2014).
(E) qPCR confirmation of *uCCNE1* and *pCCNE1* expression in four distinct clones derived from the lab's own retroviral pMIG-OSKM polycistronic construct (three technical replicates) (error bar, s.d.).
(F-G) qPCR of (F) *uCCNE1* and (G) *pCCNE1* in D551 fibroblasts 11 days after infection with

OSKM, uCCNE1, pCCNE1, or empty vector retrovirus. N.I. denotes non-infected fibroblasts. (error bar, s.d.).
(H) A model of regulation of *pCCNE1*.
(I) Validation of (Figure 3H) by double SSEA4/ TRA160 staining of reprogrammed cells. Right panel represents immunofluorescence with SSEA4 and TRA160 in hiPSC colonies generated after pCCNE1 overexpression (two biological replicates).
(J) ASE in polycistronic vector-based iPSC reprogramming (Friedli et al., 2014).

Figure S4. Effect of NOTCH signaling on iPSC reprogramming.
(A) Schematic representation of the reprogramming experiments to determine the effect of NOTCH inhibitor DAPT or NOTCH activation ligand DLL4 during different stages of reprogramming.
(B-C) The count difference of AP stained colonies in (B) DAPT- and (C) DLL4- treated cells from non-treated cells. Black, red, and blue represent treatment at whole, early, and late time points, respectively.

Figure S5. Relationship between type III/iPSC signatures and endogenous OCT4 and SOX2.
(A) GO analysis in three main principle components (PC1, 2, and 3). In each PC, top and bottom 500 genes ranked by factor loading were used for GO analysis. Dashed line represents 0.05 FDR.
(B) Venn diagram showing target genes of NANOG, PRDM14, and LIN28A.
(C) Percentage of NANOG target genes in fibroblast-type I, type II, and type III-ESC/iPSC groups (* $p < 0.05$ by hypergeometric test).
(D) Endogenous OSKM expression patterns during mouse iPSC reprogramming.
(E) Ratios of target genes by OSKM in fibroblast and type I, type II, and type III and ESC/iPSC. Gene sets are shown by pie chart.

Supplemental Figure 1

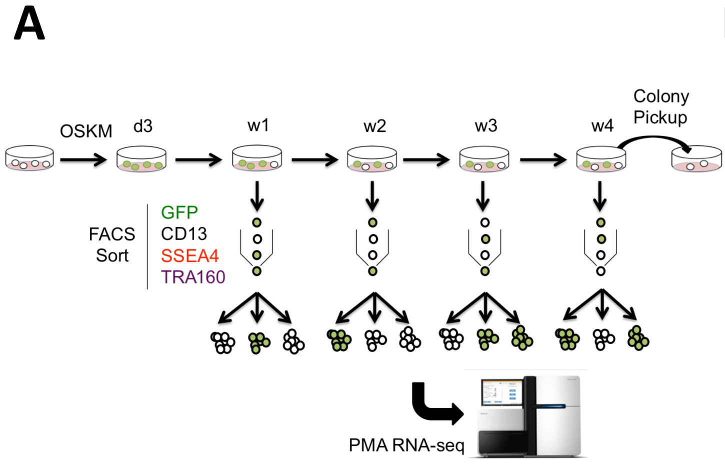

B

Date	Markers				Percentage of cell population	# of collected cells (x10^4)
	GFP	CD13	SSEA4	TRA160		
Week 1	+	-	NA	NA	4.00%	4.1
Week 1	+	+	NA	NA	72.10%	27.6
Week 2	+	-	-	NA	36.48%	10
Week 2	-	-	+	NA	8.14%	1.4
Week 2	+	-	+	NA	1.28%	3.2
Week 2	+	+	-	NA	38.16%	20
Week 2	+	+	+	NA	4.08%	10.5
Week 3	+	NA	-	-	75.41%	10
Week 3	-	NA	+	-	1.91%	2.7
Week 3	+	NA	+	-	2.80%	4.8
Week 3	-	NA	+	+	5.11%	23.2
Week 4	+	NA	-	-	43.75%	10
Week 4	-	NA	+	-	12.61%	10
Week 4	+	NA	+	-	0.48%	1.5
Week 4	-	NA	+	+	4.30%	24

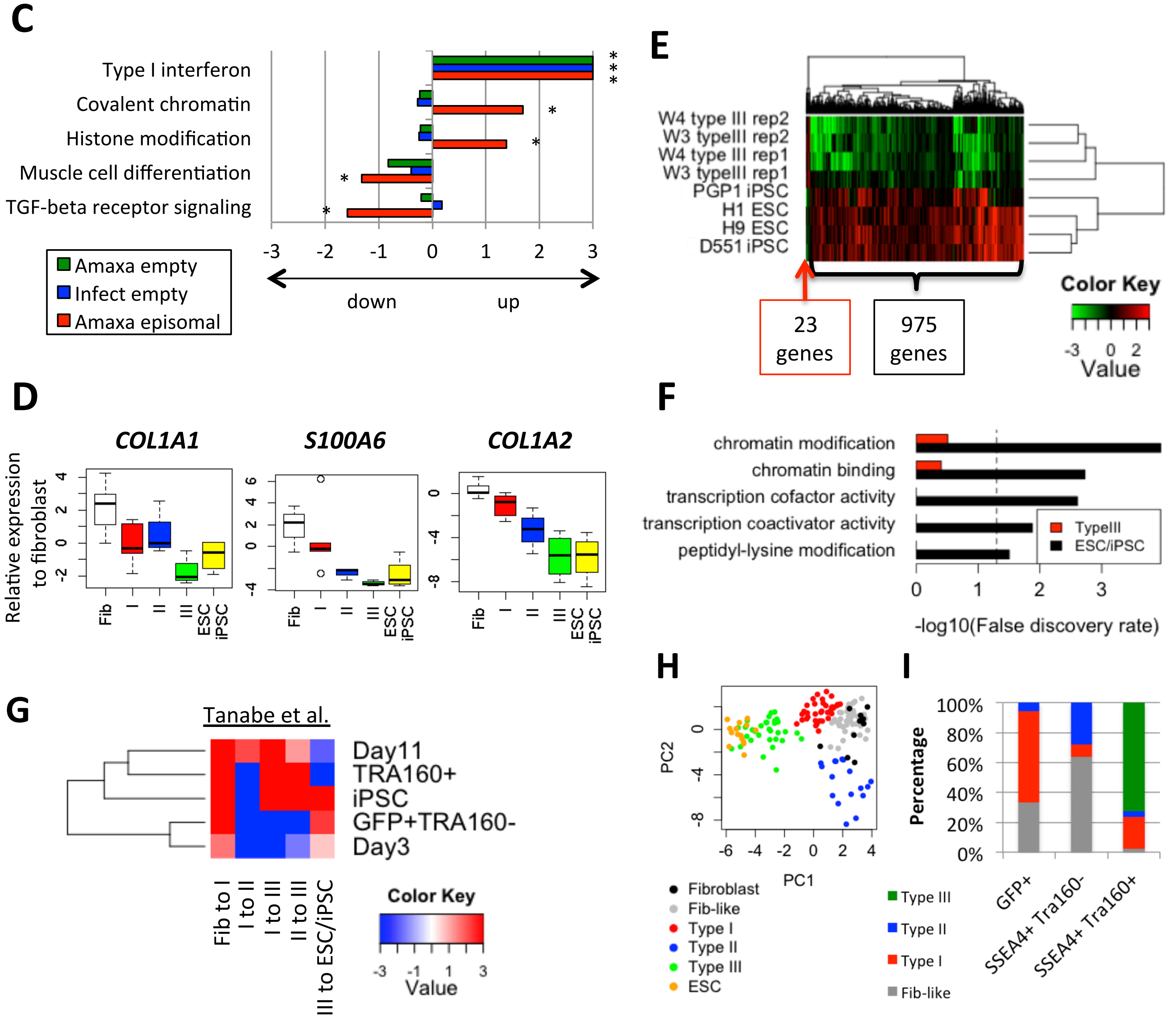

Supplemental Figure 2

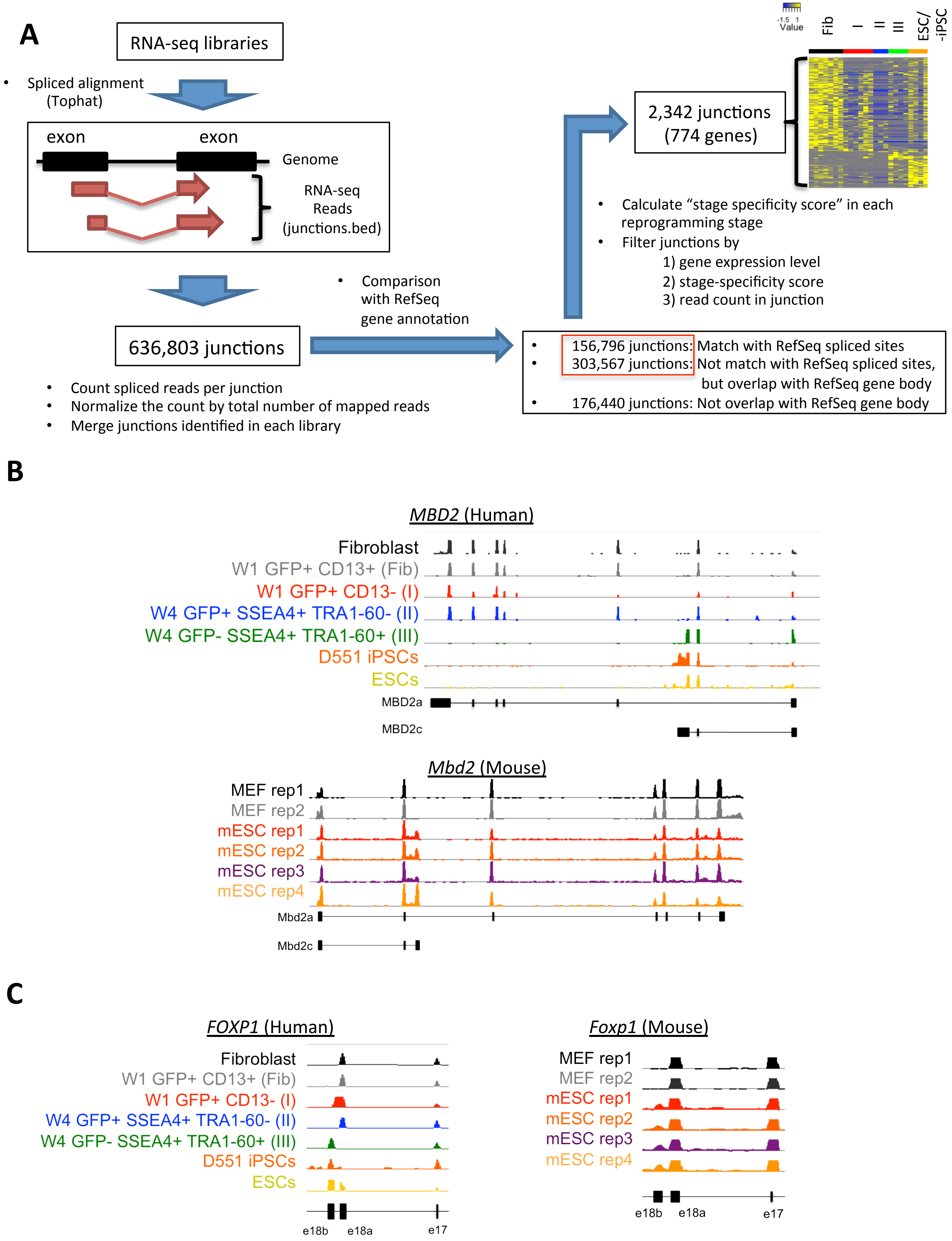
A
RNA-seq libraries
• Spliced alignment (Tophat)
exon
exon
Genome
RNA-seq Reads (junctions.bed)
636,803 junctions
• Count spliced reads per junction
• Normalize the count by total number of mapped reads
• Merge junctions identified in each library
• Comparison with RefSeq gene annotation
• 156,796 junctions: Match with RefSeq spliced sites
• 303,567 junctions: Not match with RefSeq spliced sites, but overlap with RefSeq gene body
• 176,440 junctions: Not overlap with RefSeq gene body
• Calculate "stage specificity score" in each reprogramming stage
• Filter junctions by
1) gene expression level
2) stage-specificity score
3) read count in junction
2,342 junctions (774 genes)
-1.5 1
Value
Fib
I
II
III
ESC/-iPSC
B
MBD2 (Human)
Fibroblast
W1 GFP+ CD13+ (Fib)
W1 GFP+ CD13- (I)
W4 GFP+ SSEA4+ TRA1-60- (II)
W4 GFP- SSEA4+ TRA1-60+ (III)
D551 iPSCs
ESCs
MBD2a
MBD2c
Mbd2 (Mouse)
MEF rep1
MEF rep2
mESC rep1
mESC rep2
mESC rep3
mESC rep4
Mbd2a
Mbd2c
C
FOXP1 (Human)
Fibroblast
W1 GFP+ CD13+ (Fib)
W1 GFP+ CD13- (I)
W4 GFP+ SSEA4+ TRA1-60- (II)
W4 GFP- SSEA4+ TRA1-60+ (III)
D551 iPSCs
ESCs
e18b
e18a
e17
Foxp1 (Mouse)
MEF rep1
MEF rep2
mESC rep1
mESC rep2
mESC rep3
mESC rep4
e18b
e18a
e17

Supplemental Figure 3

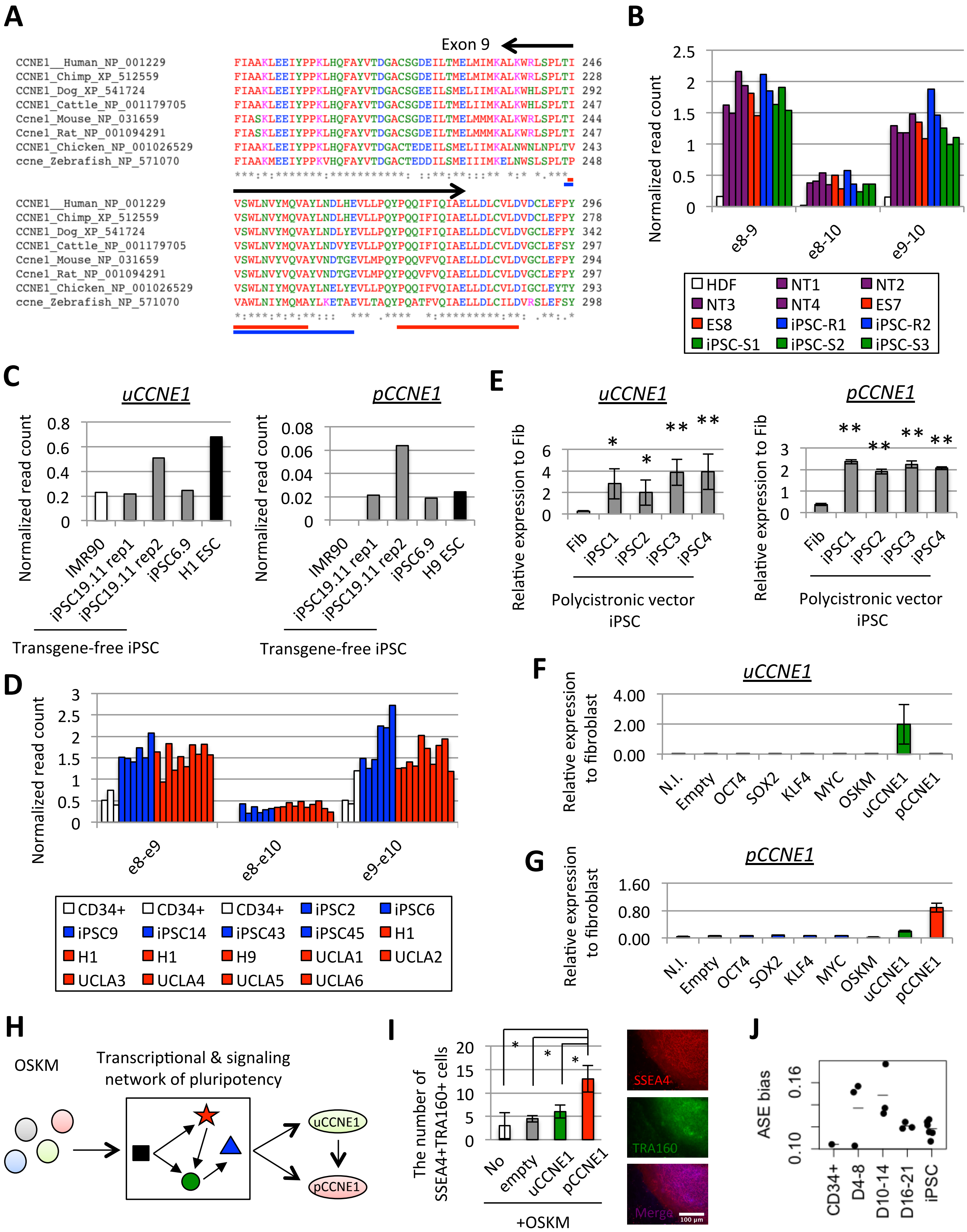

Supplemental Figure 4

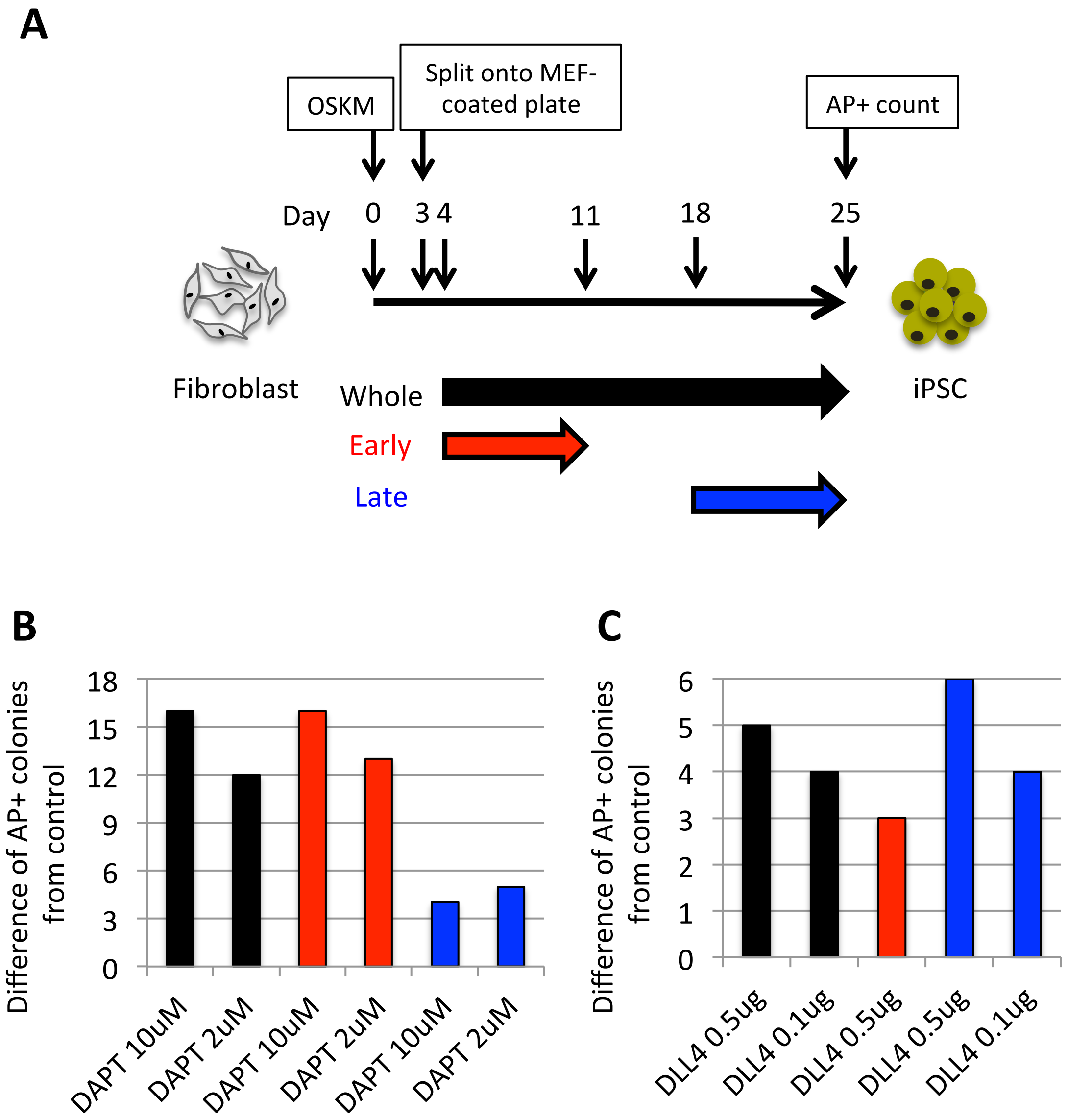

Supplemental Figure 5

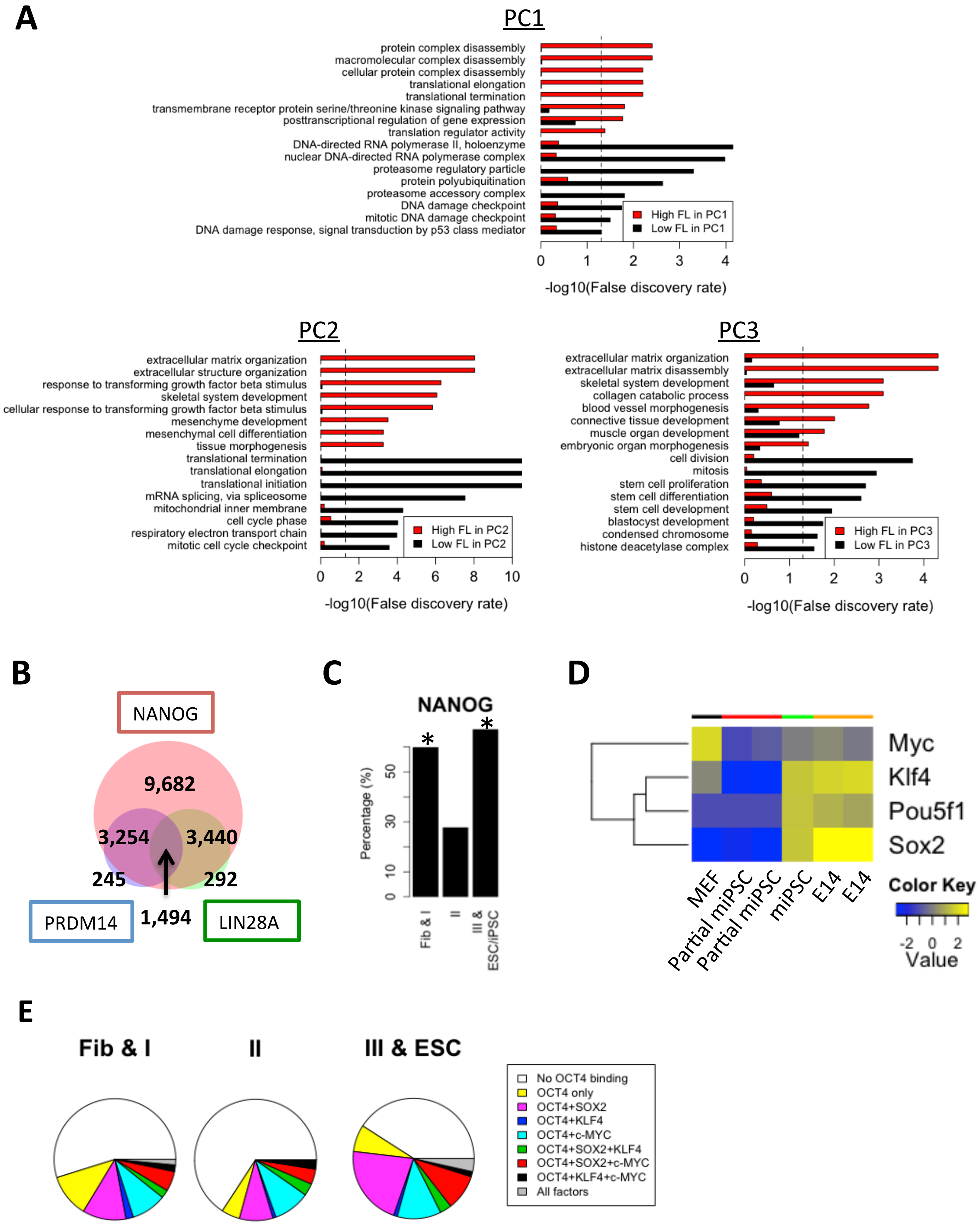

SUPPLEMENTAL TABLES

Table S1. List of differentially-expressed genes between type III and ESC/iPSC stages
Table S2. Gene sets used for GSEA in (A) Tanabe et al. datasets, (B) stem cell functions, (C) signaling pathways, and (D) cancer-related genes
Table S3 List of genes in fibroblast-type I, type II, and type III-ESC/iPSC groups
Table S4. List of endogenous OSKM-specific regions
Table S5. Summary of public ChIP-seq and RNA-seq data used in this study
Table S6. List of primer sets used in this study

SUPPLEMENTAL EXPERIMENTAL PROCEDURES

Cell culture. Detroit 551 fibroblasts (ATCC CCL110) were maintained in DMEM high glucose (Gibco) supplemented with 10% FBS and penicillin/streptomycin. Human ESCs and iPSCs were cultured on irradiated murine embryonic feeder cells (Millipore), and stem cell medium composed of DMEM/F12, 20% knockout serum replacement, 2mM non-essential amino acids, 2mM L-glutamine, 4ng/ml bFGF, and 0.1mM 2-mercaptoethanol. Retrovirus production was carried out as previously described (Park et al., 2008). OCT4, SOX2, KLF4, and c-MYC, cloned into the pMIG retrovirus backbone, were transfected individually along with pCMV-Gag-Pol, pCMV-VSVG, and the transfection reagent X-tremeGENE 9 (Roche) in 293T cells. The supernatant was collected at 24, 48, and 72 hours post-transfection, and spun at 23 000 rpm for 1.5 hours. The virus pellet was dissolved in DMEM medium followed by titration in 293T cells.

iPSC reprogramming and cell sorting. The reprogramming procedure was conducted as previously described (Park et al., 2008). Detroit 551 cells were seeded at 100 000 cells/well of a 6-well plate one day prior to infection. A retrovirus cocktail containing OCT4, SOX2, KLF4, and c-MYC was added to each well at MOI 5. The next day cells were washed 3 times with 1X PBS. On day 5-post infection, the cells were trypsinized and transferred into 10-cm culture dishes containing MEFs. One day later the medium was switched to KSR-based ESC medium and subsequently changed every other day. Prior to sorting the cells were detached using accutase, washed, and incubated in 20% FBS in 1X PBS with the following antibodies, according to manufacturer's recommended dilutions: anti-human CD13 (BD cat.# 555394), anti-human/mouse SSEA4 (R&D cat.# FAB1435A), anti-human TRA160 (BD cat.# 560193). Sorting was conducted using a BD FACSAria cell sorter. Then the cells were pelleted and quickly frozen in liquid nitrogen, or sorted directly in RLT + 2-mercaptoethanol lysis buffer (Qiagen).

PMA RNA-seq library construction and Illumina sequencing. RNA was isolated from each intermediate population as well as D551 parental fibroblasts, iPSCs derived from PGP1 and D551 fibroblasts, and H1 and H9 ESCs. PMA RNA-seq library was prepared as previously described (Pan et al., 2013). Briefly, the cells were collected, washed and stored at -80 °C as pellet before processing. RNA was isolated using RNeasy Plus Micro Kit (Qiagen cat.# 74034). Then single stranded cDNA was transcribed using Superscript III in the presence of carrier RNA (Life Technologies cat.# 18080-051). Double-stranded cDNA was generated by using the above single-stranded reaction (unpurified) in the presence of E. Coli DNA Polymerase I, E.Coli DNA Ligase, and RNaseH. The reaction was purified in the presence of carrier DNA (Zymogen cat.# D4013) prior to the ligation reaction involving end-repair enzymes and T4 DNA ligase (End-It, Epicentre cat.# ER0720). Finally, the circularized double-stranded DNA product was amplified using Phi29 DNA polymerase (Epicentre cat.# RH031110), followed by gel purification. The product was then sonicated, and library preparation conducted using standard Tru-Seq Illumina kits, followed by sequencing in HiSeq 2000.

Data processing of RNA-seq. Human genomic sequence and RefSeq gene coordinate (version hg19) were downloaded from the UCSC genome browser. All RNA-seq reads were aligned to human reference genome (hg19) by Tophat (v2.0.10) using SAMtools (v0.1.18) and Bowtie (v2.1.0) with default parameters (Trapnell et al., 2009). Unmapped reads were trimmed from 3'end and the first 50bp retained to remove error-prone 3'end. These trimmed reads were mapped to the human genome by Tophat again, and results from the first and second round mapping were merged. Then, Cufflinks (v1.2.1) was run to calculate Fragments Per Kilobase of exon model per Million mapped fragments (FPKM) by using RefSeq genes as reference annotation with "-G" option (Trapnell et al., 2010). PCA was performed to log2-transformed FPKM of 12,573 genes, which average FPKM values more than 1. Factor loading values were used to classify genes into three classes: fib/type I (PC1<0.2 and PC3>0.4), type II (PC1>0.2, PC2>-0.5 and PC3>0) and type III/ESC/iPSC-enriched genes (PC1<0.2 and (PC2+PC3)/2<-0.4). GO analysis was performed by hyperGTest function in GOstats in the Bioconductor package. Multiple-test correction was adjusted by Benjamini & Hochberg (BH) method using p.adjust function in R. The enrichment of signaling pathways and developmental genes was analyzed by GSEA (v2.0.14) software (Subramanian et al., 2005). Parameters for GSEA were set as 100 permutations of gene sets, classic enrichment statistic and signal-to-noise separation metric. 0.05 FDR was used as a cutoff for statistical significance. Gene sets used in this study were collected from public microarray data, databases and literature (Table S2).

Public microarray data analysis. Five microarray experiment data (GSE59435, GSE15603, GSE42379, GSE47489, and GSE18691) were used in this study (Chang et al., 2010; Hanna et al., 2009; Polo et al., 2012; Tanabe et al., 2013; Theunissen et al., 2014). Probe sets not overlapped with Refseq genes were removed, and those in same Refseq genes were collapsed by average. Differentially-expressed genes were identified with more than 3-fold changes and less than 0.05 FDR by T test and BH method. The datasets GSE59435 and GSE15603 were used to generate "naïve high" and "primed high" gene sets by comparison between naïve and primed ESC/iPSC in human and mouse, respectively (Table S2B). In Tanabe et al. dataset, "day3" was up-regulated genes at day 3 from fibroblasts. The datasets of "day11" was identified by comparison to the day 3 dataset, and "iPSC" was compared to day 11. All other gene sets were obtained from comparison to fibroblasts (Table S2A). Polo et al. dataset was used to compare the induction of stem cell function and signaling pathways during iPSC reprogramming in mouse (Fig. 2C and S3B). Chang et al. dataset was used to get ECC and ESC-specific genes in mouse.

Single-cell transcriptional analysis. Single cell gene expression data for fibroblasts, ESCs, and intermediate cells sorted by GFP$^+$, SSEA4$^+$TRA1-60$^-$ and SSEA4$^+$TRA1-60$^+$ were obtained from (Chung et al., 2014). Expression profiles were transformed to z-score in each cell, and then visualized by PCA. K-means clustering was performed to all intermediate cells with "centers=4" by kmeans function in R. Clusters, which are the nearest to fibroblasts and ESCs, were defined as fibroblast-like and type III group, respectively. A cluster between fibroblast-like and type III was categorized into type I. The farthest cluster from ESCs was classified into type II group.

Histone modification data analysis. Raw sequence data of ChIP-seq for H3K4me3, H3K27ac, H3K27me3 and H3K9me3 in fibroblast cells were downloaded from NCBI Short Read Archive (SRA) (Bernstein et al., 2010). ChIP-seq reads were mapped to hg19 genome by Bowtie2 with options "--local -D 15 -R 3 -N 1 -L 20 -i S,1,0.50 -k 1". The number of ChIP-seq reads in TSS±500bp was counted and then normalized by the total number of uniquely-mapped ChIP-seq reads to the genome. SRA IDs of ChIP-seq data used in this study were summarized in Table S5A.

Transcription factors and LIN28 target analysis. ChIP-seq raw data for initial binding of

OSKM in fibroblasts and OSKM, NANOG and PRDM14 in ESCs were obtained from NCBI SRA (Chia et al., 2010; Kunarso et al., 2010; Lister et al., 2009; Soufi et al., 2012). After mapping to hg19 genome by Bowtie2, their binding sites were identified by MACS2 peak caller with options "-g hs -q 0.05" (Feng et al., 2012). Refseq genes including transcription factor binding sites within 15k bp upstream and gene body regions were selected as targets. LIN28A binding sites in ESCs (GSM980593) were obtained from NCBI Gene Expression Omnibus (GEO) and reassigned from hg18 to hg19 using liftOver program (Wilbert et al., 2012). RefSeq genes including at least one LIN28A binding site in exons were selected as LIN28A targets. Overrepresentation of target genes in fibroblast-type I, type II and type III-ESC/iPSC gene group was evaluated by hypergeometric test with phyper function in R.

Analysis of endogenous OSKM. Endogenous OSKM gene expression was calculated using count of RNA-seq reads mapped to regions, which are not included in ectopic OSKM mRNA (Table S4). RNA-seq reads covering at least three base pairs in these regions were defined as endogenous OSKM-derived reads. The number of endogenous OSKM-derived reads was then normalized by total count of mapped reads. For endogenous OSKM analysis in mouse, we used RNA-seq data in MEFs, E14 mESCs, two partially-reprogrammed cells and a fully reprogrammed iPSC (Klattenhoff et al., 2013) (Table S5B).

Alternative splicing analysis. First, all splice junctions detected by Tophat were merged from all RNA-seq libraries (Fig. S2A). In each library, the number of spliced reads was counted at each splice junction and normalized by total number of mapped reads. In this study, splice junctions outside of RefSeq gene bodies were removed from subsequent analysis as part of novel transcripts or noises. To evaluate stage specificity of alternative splicing, we measured Jensen-Shannon (JS) divergence between the splice junction expression pattern and an extreme case of stage-specific expression, relying on (Cabili et al., 2011). Briefly, at each splice junction, the normalized read count *r* of library *i* were transformed to a density *r'* as:

$$r'_i = \frac{\log_2\left(r_i+1\right)}{\sum_{j=1}^{n}\log_2\left(r_j+1\right)}$$

$$r = \left(r_1, r_2, \ldots, r_n\right)$$

$$r' = \left(r'_1, r'_2, \ldots, r'_n\right)$$

where *n* is the number of RNA-seq libraries. The extreme case of stage-specific expression *e* was represented as:

$$e^S = \left(e_1^S, e_2^S, \ldots, e_n^S\right)$$

$$e_i^S = \left\{ \begin{array}{ll} \dfrac{1}{k} & if\, i \in S \\ 0 & if\, i \notin S \end{array} \right\}$$

where *k* is the number of RNA-seq libraries belonging to stage *S*. Then, the JS divergence was calculated from Shannon entropy for each intermediate stage *S* as:

$$JS(S) = H\left(\frac{r'+s}{2}\right) - \frac{H(r') + H(s)}{2}$$

$$H(p) = -\sum_{i=1}^{n} p_i \log(p_i)$$

Finally, the stage specificity score was defined as:

$$Score(S) = 1 - \sqrt{JS(S)}$$

The stage specificity score, gene expression level, and average of the normalized read count were compared with all-pairwise comparison of five reprogramming stages. Finally, as AS candidates, we selected splice junctions, satisfying the following: 1) the difference of the stage specificity score is more than 0.35, 2) average gene expression level of both stages are more than 5 FPKM, and 3) the normalized read count of at least one compared intermediate population pair is more than 1 for one pair member and less than 0.05 for the other.

Expression of *CCNE1* splicing variants was measured by read counts mapped to exon8-exon9, exon9-exon10 (*uCCNE1*), and exon8-exon10 (*pCCNE1*) junctions. The count was normalized to the total number of mapped reads. The splicing pattern of *CCNE1* was also tested in mESC, mEpiSC, nuclear transfer human stem cell, Sendai virus-derived hiPSCs and polycistronic vector-derived hiPSCs using RNA-seq data from independent groups (Factor et al., 2014; Friedli et al., 2014; Ma et al., 2014; Yu et al., 2014). We also performed qPCR confirmation of *uCCNE1* and *pCCNE1* expression in parental D551 fibroblast and four hiPSC clones generated by in-house polycistronic pMIG vector (pMIG-4F).

We also tested CCNE1 splicing in transgene-free hiPSCs by public RNA-seq data (Lister et al., 2011). Since their read size is short (<50bp), we measured the expression level of *CCNE1* variants by a different approach. First, we built an index file from a fasta file including cDNA sequences of *uCCNE1* and *pCCNE1* by bowtie-build (v0.19.7). Then, we mapped RNA-seq read to the cDNA sequence with exact matching by bowtie ("-v 0 --sam -m 1 -a --best --strata" option). The normalized count of uniquely mapped reads to total number of reads was measured as expression level of each variant.

cDNA cloning and lentivirus construction. *CCNE1* isoforms (*pCCNE1* and *uCCNE1*) were PCR amplified from H9 ESC cDNA with primers containing restriction sites of EcoRI and XhoI (Table S6) using Quick-Load® Taq 2X Master Mix (NEB, cat.# M0271S). Each isoform was purified by 2% agarose gel and Zymoclean™ Gel DNA Recovery Kit (Zymo Research, cat.# D4002). Purified cDNA was cloned into the pMIG vector, and confirmed by Sanger sequencing. For retrovirus production, each clone was transfected along with pCMV-Gag-Pol, pCMV-VSVG into HEK293T cells with 70-80% confluence at a ratio of 2:1:1.5, together with X-tremeGENE 9. The medium was changed one day after transfection, and then collected at 48 and 72 hours post-transfection. After filtration and concentration, the retrovirus was titrated and drug selected in 293T cells prior to use.

Reprogramming with CCNE1 variant. D551 fibroblast cells were seeded at 25 000 cells/well in 12-well plate before the experiment. Fibroblasts were infected with OSKM retrovirus cocktail and either empty vector, pMIG-uCCNE1, or pMIG-pCCNE1 retrovirus with MOI 5, and cultured as described above. After four weeks, the cells were fixed and stained the using Alkaline Phosphatase (AP) Assay Kit (Sigma-Aldrich cat.# 86R-1KT). Immunostaining was also performed by adding anti-SSEA4 (BD Pharmingen, cat.# 560218) and anti-TRA160 (BD

Pharmingen, cat.# 560173) antibodies for 1 hour at 4 °C. Then, the cells were washed with PBS three times. Colonies stained with both markers were counted under a fluorescence microscope.

Allele-specific gene expression analysis. For estimation of allelic bias in the intermediate states, potential variant sites were first called from each RNA-seq mapping result using *mpileup* command in SAMtools with "-Bugf" options and *view* command in BCFtools (v0.1.17) with "-bvcg" options. Resultant variations were filtered by *varFilter* command in vcfutils.pl script with default parameters. Indel, deletion or more than two alternate non-reference alleles were removed from subsequent ASE analyses. Variant sites covered by all D551 samples were used to calculate ASE ratio as following formula:

$$ASE\,ratio = \frac{(Count\,of\,reads\,with\,nonreference\,allele)}{(Count\,of\,reads\,with\,reference\,allele)+(Count\,of\,reads\,with\,nonreference\,allele)}$$

Variant sites with more than 0.8 or less than 0.2 average ASE ratio were removed as sequence errors or mutant gene expression from a small cell population. The bias of ASE is also measured as averaged absolute value of the difference between ASE ratio and 0.5.

SNP expressions of *RPN* and *P4HB* were identified by PCR amplification of cDNA (Quick-Load® Taq 2X Master Mix). Primers were designed in exon-exon junctions to avoid contamination of genomic DNA (Table S6). Amplified cDNA was subjected to Sanger sequencing in the Keck DNA Sequencing Facility at Yale School of Medicine.

For validation of ASE in polycistronic vector-derived iPSC reprogramming, we analyzed RNA-seq data from (Friedli et al., 2014) in the same manner.

Electroporation Amaxa® Cell Line Optimization Nucleofector® Kit was used to electroporate plasmid into human D.551 cells with the nucleofector device program A-023. Either pMIG empty (5 µg), pMIG-OSKM (5 µg), or episomal plasmid DNA (11ug) was electroporated into 10^6 fibroblasts. Episomal vectors oriP/EBNA1used were from (Yu et al., 2009) as follows:
pCEP4-M2L containing MYC and LIN28 (2 µg)
pEP4EO2 SET2K containing OCT4, SOX2, and KLF4 (3 µg)
pEP4EO2 SEN2K containing OCT4, SOX2, NANOG, and KLF4 (3 µg)

SUPPLEMENTAL REFERENCES

Bernstein, B.E., Stamatoyannopoulos, J.A., Costello, J.F., Ren, B., Milosavljevic, A., Meissner, A., Kellis, M., Marra, M.A., Beaudet, A.L., Ecker, J.R.*, et al.* (2010). The NIH Roadmap Epigenomics Mapping Consortium. Nat Biotechnol *28*, 1045-1048.

Cabili, M.N., Trapnell, C., Goff, L., Koziol, M., Tazon-Vega, B., Regev, A., and Rinn, J.L. (2011). Integrative annotation of human large intergenic noncoding RNAs reveals global properties and specific subclasses. Genes Dev *25*, 1915-1927.

Chang, G., Miao, Y.L., Zhang, Y., Liu, S., Kou, Z., Ding, J., Chen, D.Y., Sun, Q.Y., and Gao, S. (2010). Linking incomplete reprogramming to the improved pluripotency of murine embryonal carcinoma cell-derived pluripotent stem cells. PLoS One *5*, e10320.

Chia, N.Y., Chan, Y.S., Feng, B., Lu, X., Orlov, Y.L., Moreau, D., Kumar, P., Yang, L., Jiang, J., Lau, M.S.*, et al.* (2010). A genome-wide RNAi screen reveals determinants of human embryonic stem cell identity. Nature *468*, 316-320.

Chung, K.M., Kolling, F.W., Gajdosik, M.D., Burger, S., Russell, A.C., and Nelson, C.E. (2014). Single cell analysis reveals the stochastic phase of reprogramming to pluripotency is an ordered probabilistic process. PLoS One *9*, e95304.

Factor, D.C., Corradin, O., Zentner, G.E., Saiakhova, A., Song, L., Chenoweth, J.G., McKay, R.D., Crawford, G.E., Scacheri, P.C., and Tesar, P.J. (2014). Epigenomic comparison reveals activation of "seed" enhancers during transition from naive to primed pluripotency. Cell Stem Cell *14*, 854-863.

Feng, J., Liu, T., Qin, B., Zhang, Y., and Liu, X.S. (2012). Identifying ChIP-seq enrichment using MACS. Nat Protoc *7*, 1728-1740.

Friedli, M., Turelli, P., Kapopoulou, A., Rauwel, B., Castro-Díaz, N., Rowe, H.M., Ecco, G., Unzu, C., Planet, E., Lombardo, A.*, et al.* (2014). Loss of transcriptional control over endogenous retroelements during reprogramming to pluripotency. Genome Res *24*, 1251-1259.

Hanna, J., Markoulaki, S., Mitalipova, M., Cheng, A.W., Cassady, J.P., Staerk, J., Carey, B.W., Lengner, C.J., Foreman, R., Love, J.*, et al.* (2009). Metastable pluripotent states in NOD-mouse-derived ESCs. Cell Stem Cell *4*, 513-524.

Klattenhoff, C.A., Scheuermann, J.C., Surface, L.E., Bradley, R.K., Fields, P.A., Steinhauser, M.L., Ding, H., Butty, V.L., Torrey, L., Haas, S.*, et al.* (2013). Braveheart, a long noncoding RNA required for cardiovascular lineage commitment. Cell *152*, 570-583.

Kunarso, G., Chia, N.Y., Jeyakani, J., Hwang, C., Lu, X., Chan, Y.S., Ng, H.H., and Bourque, G. (2010). Transposable elements have rewired the core regulatory network of human embryonic stem cells. Nat Genet *42*, 631-634.

Lister, R., Pelizzola, M., Dowen, R.H., Hawkins, R.D., Hon, G., Tonti-Filippini, J., Nery, J.R., Lee, L., Ye, Z., Ngo, Q.M.*, et al.* (2009). Human DNA methylomes at base resolution show widespread epigenomic differences. Nature *462*, 315-322.

Lister, R., Pelizzola, M., Kida, Y.S., Hawkins, R.D., Nery, J.R., Hon, G., Antosiewicz-Bourget, J., O'Malley, R., Castanon, R., Klugman, S.*, et al.* (2011). Hotspots of aberrant epigenomic reprogramming in human induced pluripotent stem cells. Nature *471*, 68-73.

Ma, H., Morey, R., O'Neil, R.C., He, Y., Daughtry, B., Schultz, M.D., Hariharan, M., Nery, J.R., Castanon, R., Sabatini, K.*, et al.* (2014). Abnormalities in human pluripotent cells due to reprogramming mechanisms. Nature *511*, 177-183.

Pan, X., Durrett, R.E., Zhu, H., Tanaka, Y., Li, Y., Zi, X., Marjani, S.L., Euskirchen, G., Ma, C., Lamotte, R.H., *et al.* (2013). Two methods for full-length RNA sequencing for low quantities of cells and single cells. Proc Natl Acad Sci U S A *110*, 594-599.

Park, I.H., Lerou, P.H., Zhao, R., Huo, H., and Daley, G.Q. (2008). Generation of human-induced pluripotent stem cells. Nat Protoc *3*, 1180-1186.

Polo, J.M., Anderssen, E., Walsh, R.M., Schwarz, B.A., Nefzger, C.M., Lim, S.M., Borkent, M., Apostolou, E., Alaei, S., Cloutier, J., *et al.* (2012). A molecular roadmap of reprogramming somatic cells into iPS cells. Cell *151*, 1617-1632.

Soufi, A., Donahue, G., and Zaret, K.S. (2012). Facilitators and impediments of the pluripotency reprogramming factors' initial engagement with the genome. Cell *151*, 994-1004.

Subramanian, A., Tamayo, P., Mootha, V.K., Mukherjee, S., Ebert, B.L., Gillette, M.A., Paulovich, A., Pomeroy, S.L., Golub, T.R., Lander, E.S., *et al.* (2005). Gene set enrichment analysis: a knowledge-based approach for interpreting genome-wide expression profiles. Proc Natl Acad Sci U S A *102*, 15545-15550.

Tanabe, K., Nakamura, M., Narita, M., Takahashi, K., and Yamanaka, S. (2013). Maturation, not initiation, is the major roadblock during reprogramming toward pluripotency from human fibroblasts. Proc Natl Acad Sci U S A *110*, 12172-12179.

Theunissen, T.W., Powell, B.E., Wang, H., Mitalipova, M., Faddah, D.A., Reddy, J., Fan, Z.P., Maetzel, D., Ganz, K., Shi, L., *et al.* (2014). Systematic Identification of Culture Conditions for Induction and Maintenance of Naive Human Pluripotency. Cell Stem Cell.

Trapnell, C., Pachter, L., and Salzberg, S.L. (2009). TopHat: discovering splice junctions with RNA-Seq. Bioinformatics *25*, 1105-1111.

Trapnell, C., Williams, B.A., Pertea, G., Mortazavi, A., Kwan, G., van Baren, M.J., Salzberg, S.L., Wold, B.J., and Pachter, L. (2010). Transcript assembly and quantification by RNA-Seq reveals unannotated transcripts and isoform switching during cell differentiation. Nat Biotechnol *28*, 511-515.

Wilbert, M.L., Huelga, S.C., Kapeli, K., Stark, T.J., Liang, T.Y., Chen, S.X., Yan, B.Y., Nathanson, J.L., Hutt, K.R., Lovci, M.T., *et al.* (2012). LIN28 binds messenger RNAs at GGAGA motifs and regulates splicing factor abundance. Mol Cell *48*, 195-206.

Yu, W., McIntosh, C., Lister, R., Zhu, I., Han, Y., Ren, J., Landsman, D., Lee, E., Briones, V., Terashima, M., *et al.* (2014). Genome-wide DNA methylation patterns in LSH mutant reveals de-repression of repeat elements and redundant epigenetic silencing pathways. Genome Res.